

Espen Forseth Westrum
Kamilla Paulsen

Harvesting of kinetic energy from marine animals

A study on piezoelectric generators operating at low frequency vibrations

Bachelor's project in Electrical engineering
Supervisor: Cuong Phu Le
May 2021

Espen Forseth Westrum
Kamilla Paulsen

Harvesting of kinetic energy from marine animals

A study on piezoelectric generators operating at low
frequency vibrations

Bachelor's project in Electrical engineering
Supervisor: Cuong Phu Le
May 2021

Norwegian University of Science and Technology
Faculty of Information Technology and Electrical Engineering
Department of Electronic Systems





Institutt for elektroniske systemer

Oppgavens tittel Høsting av bevegelsesenergi fra marine dyr – <i>En studie av piezoelektriske generatorer ved lavfrekvente vibrasjoner</i>	Gitt dato 16. januar 2021
	Innlevingsdato 8. juni 2021
Project title Harvesting of kinetic energy from marine animals – <i>A study on piezoelectric generators operating at low frequency vibrations</i>	Gradering [X] åpent
	Antall sider/bilag 51/26
Gruppedeltakere Espen F. Westrum Kamilla Paulsen espenfw@stud.ntnu.no kamillimeter@gmail.com +47 980 34 391 +47 918 51 920	Veileder internt Cuong Phu Le cuong.le@ntnu.no +47 942 57 411
Studieretning Industriell Instrumentering	Prosjektnummer E2136
Oppdragsgiver Thelma Biotel AS	Kontaktperson Erik Høy +47 920 31 433

ABSTRACT



Wireless sensor networks are a hot topic in the industry of today. Their popularity is becoming more and more widespread. Unfortunately, the sensors being wireless means their reliance on batteries are present, and this reliance can in some cases become a limitation as the longevity of the sensor is directly affected. As a way of combating this reliance, different approaches to energy harvesting are being investigated as possible solutions.

The purpose of this thesis is to investigate the potential in harvesting bending or vibrational energy from fish as it swims. For this, different configurations were considered, both from a feasibility and ethical perspective. The approach chosen for this paper was using a piezoelectric cantilever to harvest the energy caused by vibrations from the tail beat.

Simulations were used to approximate the potential power output of the harvester, as well as an experimental setup to measure the real results of a commercially available piezoelectric energy harvester. To adjust the resonance frequency of the system, changes were made to the tip mass of a cantilever configuration, as well as the physical geometry of the cantilever itself.

The results show that, for a commercially available vibrational or bending energy harvester to be useful for extremely low frequencies, a great deal of configurations must be made. However, there is a potential for an energy harvester-driven sensor.

This study attempt to answer the question whether or not a piezoelectric energy harvester could power a sensor from the vibrational energy of the fish. As the study states: the most demanding challenge surrounding this approach is the low frequencies the cantilever is operating at. Although this study did not solve the problems regarding harvesting the kinetic energy from fish, it does show that the potential is there. Furthermore, the study lists a number of possible configurations and workarounds to potentially solve the technical problems surrounding the low operating frequency. Further studies are needed to establish the feasibility of using commercially available energy harvesters for more extreme ranges than is advertised. The propositions presented by this paper could lead to further breakthroughs into the field of biomechanical energy harvesting.

SAMMENDRAG



Trådløse sensornettverk er i vinden om dagen og er de siste årene blitt mer utbredt i industrien og hos forbrukere. Dette betyr også at det i dag er en hel del flere elektroniske apparater og innretninger som trenger batterier for å driftes. Denne avhengigheten kan i mange tilfeller være en flaskehals for sensorens levetid, spesielt i de tilfellene der sensoren er plassert i mindre tilgjengelige miljøer. Det er de siste årene derfor økt interesse for energihøsting, som mange tror kan være nøkkelen for en forlenget levetid for sensorer.

Denne bacheloroppgaven tar for seg energihøsting for å drifte sensorer implantert i fisk ved å høste kinetisk energi og konvertere den til elektrisk energi. Det blir vurdert forskjellige løsninger for dette, da om det er gjennomførbart og fra et etisk perspektiv. Retningen valgt i denne oppgaven baserer seg på å høste energi fra vibrasjoner som skapes når fiskens hale beveger seg frem og tilbake, ved bruk av en fleksibel piezoelektrisk cantilever.

Ved å bruke simuleringer for å approksimere den elektriske energipotensialet, i tillegg til reelle forsøk, vil det undersøkes om det er mulig å bruke kommersielt tilgjengelige energihøstere for å drive sensoren. For å tilpasse systemets resonans til frekvensene til stede i fiskens haleslag vil cantileverens utforming endres, i tillegg vil den også lastes med ulike lastmasser.

Resultatene viser at dersom kommersielt tilgjengelige energihøstere basert på vibrasjon eller bøyning skal være effektive på ekstremt lave frekvenser, er det behov for større konfigurasjoner. Når det er sagt, dersom man skulle lykkes, er potensialet for å drive sensorer med energihøstere en mulighet.

Denne studien prøver å besvare spørsmålet om piezoelektriske energihøstere kan drive en trådløs sensor, da ved å konvertere fiskens kinetiske energi til elektrisk energi. Det konkluderes med at den største utfordringer her, er å få et system til å resonere på ekstremt lave frekvensene. Selv om studien ikke har landet på en definitiv løsning, er det vist at fiskens bevegelse er en potensiell energikilde. Det listes også opp mulige tekniske løsninger for å adressere utfordringen med lave frekvenser og lav aksellerasjon. Det anmodes om videre forskning på området for å oppnå konkluderende data.



Preface

We have written this bachelor thesis on behalf of *Thelma Biotel AS* and the *Faculty of Information Technology and Electronics (IE)* at the *Norwegian University of Science and Technology (NTNU)*.

The inspiration behind this study stems from the combination of a job advert and a guest lecture on energy harvesting. The job advert was as a telemetry engineer for *Thelma Biotel AS*, and the lecture was held by none other than our much beloved supervisor, *Cuong Phu Le*.

Common ground was quickly established, and from the humble beginning of 1, the group quickly doubled in size and enthusiasm. An interesting, important and complex roller-coaster of a project started to take form. We hope that our work can inspire others to further studies.

The thesis is both written and researched by us; *Espen Forseth Westrum* and *Kamilla Paulsen*, and it represents the end and completion of a three year bachelors degree in electrical engineering (instrumentation). We have learned, laughed and struggled, and we can now proudly present our work.

Warts and all.

Acknowledgement

We wish to extend our gratitude towards our supervisor, *Cuong Phu Le* (associate professor at *NTNU*) for his continuous support, patience and technical advice during this study. We also want to thank *Erik Høy* from *Thelma Biotel AS* for his interest and eagerness to engage with the project, which exceeded our expectations.

Furthermore, we wish to give a special thanks to *Even JC*, and all the people that provided us with knowledge, data and needed equipment: *Robert Lennox*, *Martin Føre*, *Jan Davidsen*, *Ingulf Helland*, *Tim Cato Netland*, *Snorre Vestli*, *Thomas Overen*, *Stine Mari Johnsen* and *Al*.

We couldn't have done it without you.

CONTENT

ABSTRACT	VII	3.4. Test rig	15
SAMMENDRAG	IX	3.5. Experiments	17
LIST OF TABLES	XIII	4. RESULTS	19
LIST OF FIGURES	XV	4.1. Preparations	19
DEFINITIONS	XVII	4.2. Simulation	19
1. INTRODUCTION	1	4.3. Test rig	20
1.1. Background.....	1	4.4. Experiments.....	22
1.2. Objective.....	1	5. DISCUSSION	23
1.3. Preamble.....	1	5.1. About the case.....	23
1.4. Similar studies.....	2	5.2. Activity data.....	24
2. THEORY	3	5.3. Simulation.....	24
2.1. Energy harvesting.....	3	5.4. Test rig	25
2.2. Piezoelectricity.....	4	5.5. Experiments	26
2.3. Piezoelectric energy harvesters.....	6	5.6. Other challenges.....	27
3. METHOD	11	5.7. Further work.....	28
3.1. Research.....	11	5.8. Conclusion.....	30
3.2. Case.....	12	REFERENCES	33
3.3. Simulation.....	14	APPENDIX	35

LIST OF TABLES



Table 1: Symbols and units.....	XVII
Table 2: Batteries vs. super capacitors	4
Table 3: Some properties for 5H, 5A, 5J	6
Table 4: Search words and keywords.....	11
Table 5: Parameters of data set A and B	11
Table 6: Frequency and acceleration area	12
Table 7: Current and voltage requirements for WSN	12
Table 8: Geometrical parameters for the individual parts of the sensor system	13
Table 9: Analogies for the e→v model.....	14
Table 10: Simulation parameters	15
Table 11: Measurements with peak acceleration of 0.1 G.....	22
Table 12: Experiments, results from initial tests	22

LIST OF FIGURES

Figure 1: The steps of energy harvesting.....	3	Figure 19: Cantilever B with proof mass.....	16
Figure 2: Electric field from material deformation.	4	Figure 20: Accelerometer	17
Figure 3: Molecular structure of crystal.....	4	Figure 21: Proof mass used.....	17
Figure 4: Polarization of crystal domains.....	5	Figure 22: End stop and magnets on cantilever A	17
Figure 5: Different piezoelectric modes	6	Figure 23: Spectrum analysis of data set A.....	19
Figure 6: Electrode placements for mode 31 and 33.....	6	Figure 24: Frequency sweep from simulation	20
Figure 7: Common piezoelectric configuration	7	Figure 25: Simulation circuit at resonance.....	20
Figure 8: Cantilever configuration	7	Figure 26: Frequency sweep from test rig.....	21
Figure 9: Q-factor and bandwidth.....	8	Figure 27: Test rig measurements.....	21
Figure 10: Available transmitter sizes from TB	12	Figure 28: Power measurements.....	21
Figure 11: Size of chosen transmitter	13	Figure 29: Endstop and magnet experiment.....	22
Figure 12: Placements of implanted beam.....	13	Figure 30: Bending of fish tail	28
Figure 13: Cantilever and film beam.....	13	Figure 31: Spiral shaped springs.....	29
Figure 14: Cantilever inside gas filled container.....	13	Figure 32: Other possible spring shapes.....	29
Figure 15: Chosen harvester.....	14	Figure 33: Trapezoid piezoelectric beam.....	29
Figure 16: Mechanical to electrical analogies.....	15	Figure 34: Rectifier and voltage transformer	30
Figure 17: Setup of test rig.....	16	Figure 35: Triangle of expense.....	30
Figure 18: Block diagram of setup.....	16		

DEFINITIONS



Nomenclature

Attribute	Symbol	Unity	Description
Voltage	V	[V]	
Current	i	[A]	
Power	P	[W]	
Displacement	x	[mm]	
Mass	m	[kg]	
Frequency	ω	[Hz]	Angular frequency is given in Hz, not rad/s for resonance.
Frequency (natural)	ω_n	[Hz]	
Stiffness	k	[N/m]	Material property
Resistance	R	[Ω]	
Inductance	L	[H]	
Capacitance	C	[F]	
Damping	B	[Ns/m]	
Q Factor	Q	-	Quality factor. Describes the sharpness of the resonance frequency.
Coupling coefficient	K^2	-	Converted energy between mechanical and electrical domains
Acceleration	A	[G]	
Young's modulus	Y	[N/m ²]	Material property. Describes elasticity and material softness.

TABLE 1: Symbols and units.

Abbreviations

- » TB - Thelma Biotel AS
- » AC - Alternating current
- » DC - Direct current
- » PZT - Lead zirconate
- » EH - Energy harvester
- » VEH - Vibration based energy harvester
- » EMEH - Electromagnetic energy harvester
- » EEH - Electrostatic energy harvester
- » MEMS - Micro electro-mechanical system
- » PEH - Piezoelectric energy harvester
- » WSN - Wireless sensor node
- » AS - Atlantic Salmon (*Salmo Salar*)
- » FFT - Fast Fourier transform
- » MSDS - Mass-spring-damper system
- » ELF - Extremely low frequencies
- » RMS - Root mean square
- » BW - Bandwidth

1. INTRODUCTION

1.1. Background

Thelma Biotel AS

Thelma Biotel AS (TB) is a technology company based in Trondheim, Norway. They focus on telemetric surveillance of marine animals and other offshore monitoring solutions. Their solutions are mostly based around monitoring fish behavioural patterns. To achieve this, they use a technique where a *wireless sensor node (WSN)* is implanted inside of the abdominal cavity, enclosed in the tissue of the fish. The WSN can measure acceleration, pressure, temperature, roll and tilt, and they have a unique ID to tell the individuals apart from each other. As the fish swims around in the fjords, or migrate from sea to freshwater, the sensor transmits an acoustic signal. This is picked up from receivers placed on buoys where the tag data is stored for later collection [1].

Motivation

The development of battery technology can be considered one of the most important breakthroughs in modern history. The ability to store energy over longer periods of time enables almost unlimited possibilities in science, production and consumer electronics. The batteries are undoubtedly here to stay to further power the future.

Energy harvesters (EH) are promising as a concept today, and of growing interest in energy production. With the technology of today, there are only a handful of devices that have a low enough power consumption to reliably be powered by a harvester alone. In most cases the EH cannot replace batteries completely, and today they fill a rather small niche of uses, mostly in remote sensor networks. The hope is that they someday can completely erase the need for batteries, being powerful enough to drive the sensor by its own. However, for now the more feasible solution is having EH work in tandem with the batteries.

TB's transmitters are built to operate continuously, or in intervals for long periods of time. Because of their small size and minimal energy consumption, batteries can keep

sensors going for months and in some cases, years. The main deciding factor for the lifespan of a sensor today is the size of the battery. Today the sensors are driven by batteries, which works well for larger fish, but causes problems for logging the activity of the smaller fish.

1.2. Objective

Problem

The purpose of this paper is to investigate methods of harvesting energy from fish in motion, to power the WSN implanted inside the animal, and to further prove that kinetic energy can be harvested.

Approach

This is to be achieved through research, simulation, testing and hopefully prototyping, if the given time allows it. The starting point is to choose a suitable case for his very purpose, and to further investigate what can be achieved given the specification.

1.3. Preamble

Marine animal tracking

One might wonder what the purpose behind tracking is, and there are several answers to this. One of the main answers is that it allows a broader knowledge base, which is important for us to understand the behavior of different species. Furthermore, it helps us keep an oversight over the populations, which is highly motivated by the decreasing stock of many marine species. Especially when it comes to Salmonidae, where many species are red listed, see *appendix D*.

One example is the *Atlantic Salmon (AS)*, which in Europe are listed as vulnerable [2]. It is therefore important for scientists and marine biologists to have a solid information base, both on movement and other behavioral aspects.

Like other Salmonidae, the AS is anadromous, which means they migrate between freshwater and the ocean. The

juvenile AS spend their first 2-5 years in rivers or streams, and after reaching the early adult stage (smolt) they migrate to the ocean. During ocean life the AS matures and becomes fertile, before returning to spawn in freshwater (kelt). Not all individuals survive spawning, but those who do repeat the migration process [3]. Because of this migration, it would be especially valuable to track the individuals over longer periods of time

Longer sensory lifespans will provide a better data base, which can help understand and also protect endangered species.

The concept of energy

When something or someone moves, energy is created, and part of this is transferred to heat. If the energy gets lost instead of being stored and put to a more specific use, it is considered waste energy.

Because of the world's increasing energy usage, efficiency and sustainability has become a pillar for new scientific innovation, and aims to reduce energy loss.

The concept of energy loss is known from the earlier wide use of incandescent light bulbs. Most modern light sources today are LED lights, where the majority of input energy goes to light production and heat generation is therefore minimal. This makes LED light sources considerably more energy efficient than that of the predecessor.

To avoid that the energy falls under the waste term, it could be harvested and put to use. In a world where power consumption is a growing concern, the ability to utilize energy in creative ways becomes more important, thus the growing interest in the field of EH.

EH, simply put, is an umbrella term that captures all the different types of energy production. However, the term energy harvesting does carry with it some connotations in most industries and academic circles. Although the principles of energy harvesting are similar to what we would call traditional energy production, it is usually related to a lower scale for powering electronics.

As a result of the small levels of power EH can produce they have for a long time been seen as inferior sources of energy. This is also a result of the availability of cheap batteries, but as electronics become more efficient, the EH are once again sparking an interest and more research than ever before is put into the subject.

1.4. Similar studies

There are few studies that directly targets energy harvesting within the area of marine animals. Especially when it comes to the kinetic energy generated from the fish. On this specific topic, there is one paper in particular that addresses some of the same questions.

In "*An Energy Harvesting Underwater Acoustic Transmitter for Aquatic Animals*" Li et. al. found that it is possible to achieve an adequate outtake for powering a single transmitter [6].

Also, in "*Energy Harvesting from a Piezoelectric Biomimetic Fish Tail*", it was shown by Cha, Youngsu et al. that the generated output gave promising results for further research [7].

Apart from these niche studies, some of the research that have proven to be resourceful are mainly review articles on piezoelectric energy harvesters, and on piezoelectricity and energy harvesters in general.

2. THEORY

In this section, the main focus will be on the basics of *energy harvesters (EH)* and the piezoelectric effect. The purpose is to explain some of the terminology and concepts that supports this thesis.

2.1. Energy harvesting

The list of possible energy sources is long, and amongst the more frequent we find *wind, water, sunlight* and also *radio-frequency*. Another source, which has grown rapidly for the purpose of harvesting usage, is mechanical energy generated by movement and ambient vibrations [5]. As explained in the preamble, the purpose is to make use of waste energy from moving sources, that otherwise would be lost.

Harvesting technologies

There are many technologies available for harvesting usage, and their usage are determined by the energy environment and magnitude of the source.

When it comes to biomechanics, and mechanical-to-electrical energy conversion, the three most common technologies are electromagnetic, triboelectric (in the form of electrostatic) and piezoelectric [5, 8].

Electromagnetic EH (EMEH) are inductive type harvesters, with a ferromagnetic material that alters the magnetic flux. EMEH can operate at low frequencies, and are known for creating high currents, but as a result they also produce low voltages [9]. *Electrostatic EH (EEH)* on the other hand, are capacitive type harvesters, which allow greater voltages. When it comes to small scale electronics, both EMEH and EEH are inferior to that of the *piezoelectric EH (PEH)*.

PEH are considered the leading technology for *micro electro-mechanical systems (MEMS)*, as they have a high energy density [5, 8, 9], which means that they can produce a sufficient power output with a rather minimal volume. PEHs have a high voltage output and can operate over a broad frequency spectrum, and in comparison with EMEH and EEH, they are considered cost-efficient and production friendly [9]. When using PEH to transform mechanical strain from vibrations into usable energy [5, 9] it is, utmost important that this energy is stored in a sufficient way.

Energy storage

There are two scenarios for a functioning EH, see *figure 1*. Scenario A: The energy harvested is sufficient enough, and

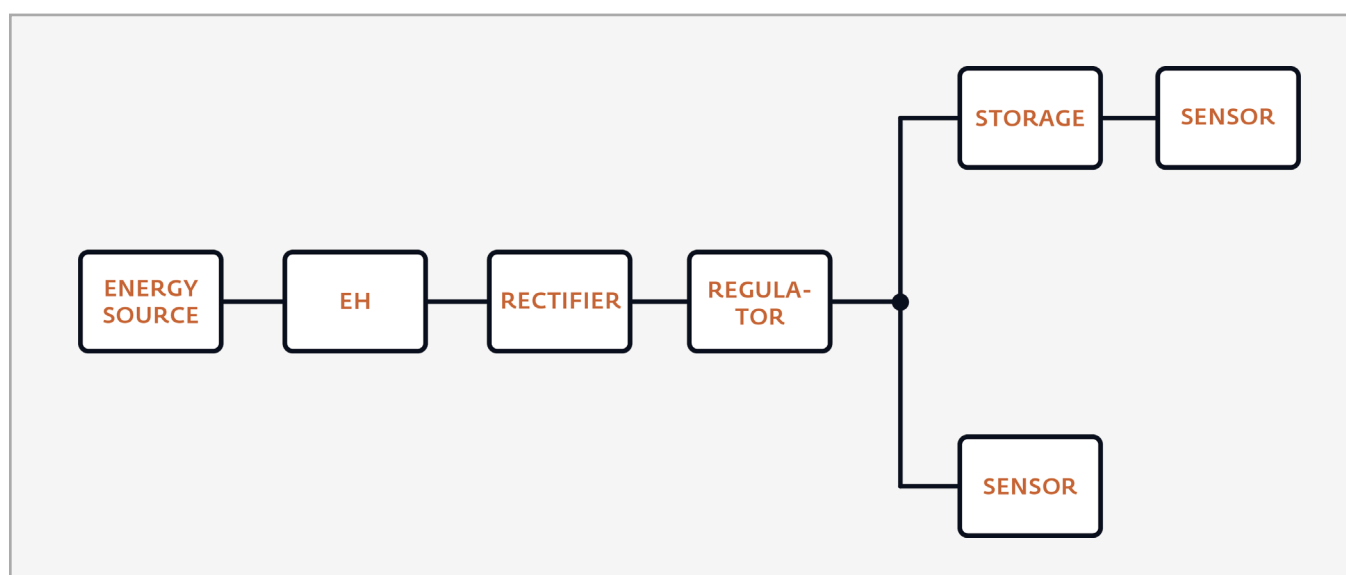


FIGURE 1: The steps of energy harvesting, with or without storage medium.

the source intense enough, to power the device directly. Scenario B: The momentary energy is not sufficient and must be stored and accumulated over time, in either a battery cell or a super capacitor. Today, the most common storage medium is batteries. Although they are preferred, they come with tradeoffs which can potentially limit the sensor's lifespan. The battery's shortened lifespan comes from the limited amount of recharge cycles the battery can perform. This problem is not as apparent for supercapacitors, which tolerates many more recharges, almost without loss in capacity. However, their difference in leakage and energy density, favor the battery [10]. See *table 2* for key distinctions between the two storage mediums.

Description	Battery	Supercapacitor
Recharge cycle lifetime	< 10 ³ cycles	> 10 ⁶ cycles
Self-discharge rate	5 %	30 %
Voltage [V]	3.7–4.2	0–2.7
Energy density [Wh/kg]	high (20–150)	low (0.8–10)
Power density [W/kg]	low (50–300)	high (400–500)
Fastest charging time	hours	sec–min
Fastest discharge time	0.3 – 3 hours	< a few min
Charging circuit	complex	simple

TABLE 2: Batteries vs. super capacitors

As most forms of generated electricity is alternating current (AC), and must therefore be converted to direct

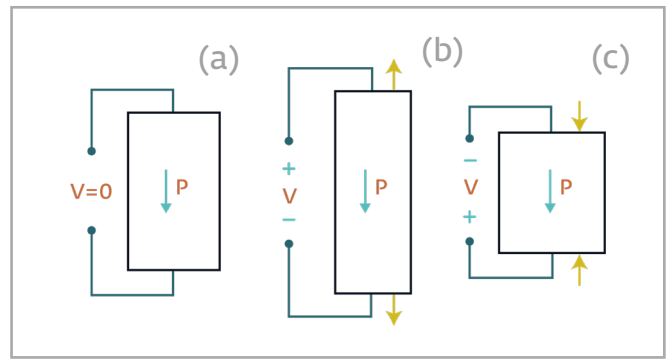


FIGURE 2: Electric field caused by material deformation. Adapted from Figure 2 (page 5) in [12].

current (DC) before it can be stored in any medium. For this a rectifier circuit is needed. There are a few different things one must consider when picking a rectifier. Remember that EHs wants as much energy as possible to transfer from the transducer to the storing medium. See *section 5.7*.

2.2. Piezoelectricity

The piezoelectric effect

The piezoelectric effect refers to mechanical-electric coupling properties of some dielectric materials. This effect can be explained as the ability of certain materials to produce an electric field from mechanical stress, or inversely, produce deflection from electrical charge.

When the material experiences deformation caused by external forces, the piezoelectric phenomenon allows the formation of an electric field. This is what is called the direct piezoelectric effect. see *figure 2*. The converse piezoelectric effect occurs when the material is subjected to an electric

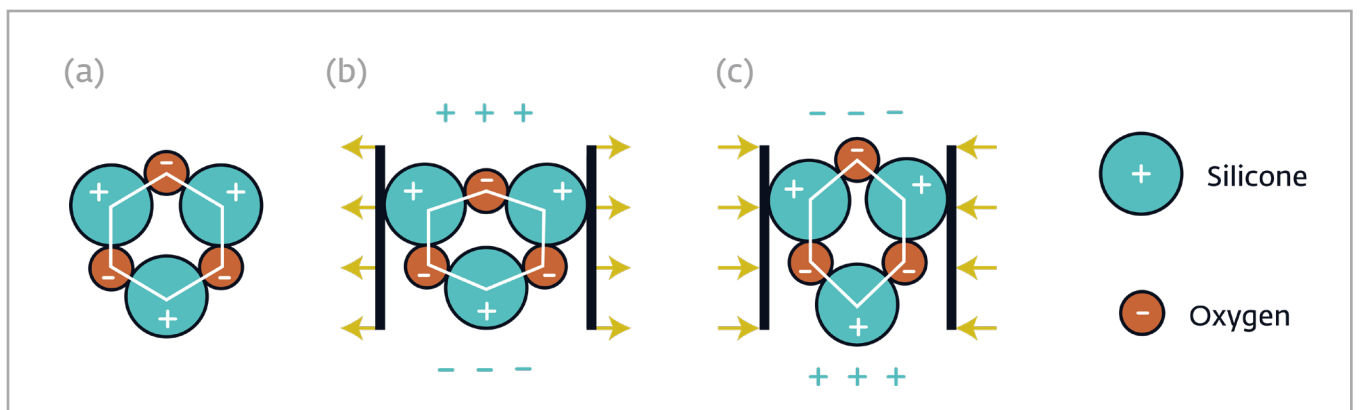


FIGURE 3: Molecular structure of crystal (a) neutral, (b) tension, and (c) contraction. Adapted from Figure 3 (page 4) in [25].

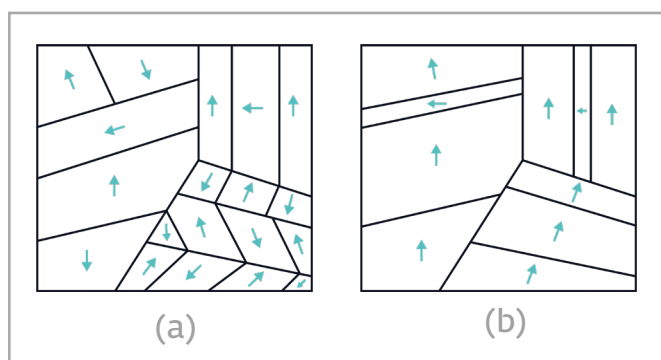


FIGURE 4: Polarization of crystal domains. Orientation is represented by arrows. (a) before polarization. (b) after polarization. Adapted from Figure 1 (page 4) in [12].

field, and therefore deforms. This converse effect is frequently used as buzzers and acoustic transmitters.

Although this phenomenon may seem extraordinary, a great deal of materials inherit these properties, but the deformation and strength of the electrical field produced will differ greatly depending on the material. The relationship is explained by:

$$[1] \quad D_e = d_j T + \epsilon_m E$$

$$[2] \quad S_m = sT + d_n E$$

Where D_e is the electric displacement, d_j is the strain coefficient, T is stress (mechanical), ϵ_m is the permittivity (given for zero mechanical stress), S_m is the strain (mechanical), s is the compliance and d_n is a piezoelectric coefficient.

The voltage produced by the piezoelectric material is proportional to both stress and strain, meaning that the greater the strain on the material, the higher the voltage is [11]. To explain how this effect occurs we need to see what happens on a molecular level.

Piezoelectric materials have a particular crystal structure. Quartz crystals (see figure 3), for instance, possess such a cage-like structure. When a force is applied and the material is compressed in any direction the net positive and negative charges are also displaced, causing the structure to polarize. When naturally occurring, the material is divided into many of these small crystal domains, each one with random orientation to neighboring domains. In these cases the piezoelectric effect will be too weak to establish

a potent electric field, since each of the domains will cancel each other out, leaving us with a zero, or close to zero potential [12].

For a piezoelectric material to be of meaningful use it needs to be artificially polarized. This process is called poling [12], and is an important ability of many ferroelectric perovskites [9].

To achieve a permanent poling the material is subjected to a strong electric field in the desired direction which will cause the crystal domains to get polarized. As a result of this, the material develops a stronger bipolar state which remain, even after the process of polarization is over. In other words, the crystal domains have been permanently deformed as shown in figure 4.

Piezoelectric transducers

The ability to permanently polarize piezoelectric material is critical for obtaining efficient EHs. As EH's will usually not achieve power greater than a few milliwatts, it is essential that they generate as much energy per unit of stress. However, the degree of polarization is not the only limiting factor when it comes to the EH's capabilities. There are other material properties as well one must consider, such as; the piezoelectric coefficients, energy density, dielectric constant and the electromechanical coupling coefficient. Indeed, the direction of displacement, related to the materials poling, also plays an important part in the efficiency of the transducer.

One of the more important piezoelectric coefficients is the coupling coefficient. The coupling coefficient (K) indicates the ratio between applied strain and electrical yield. Because of the mentioned poling the coupling coefficient will have different values depending on the direction of the poling. Known as poling modes.

$$[3] \quad K^2 = \frac{\text{electrical energy stored}}{\text{mechanical strain applied}}$$

These modes are referred to as $d_{\#\#}$, where the subscript indicates the direction of force acting upon the material. The first subscript explains which way the material is poled. The number 3 relating to the Z-axis. 1 and 2, are X and Y, respectively [13]. However 1 is usually used interchangeably with 2, and can be thought of as the normal plane to Z. The second

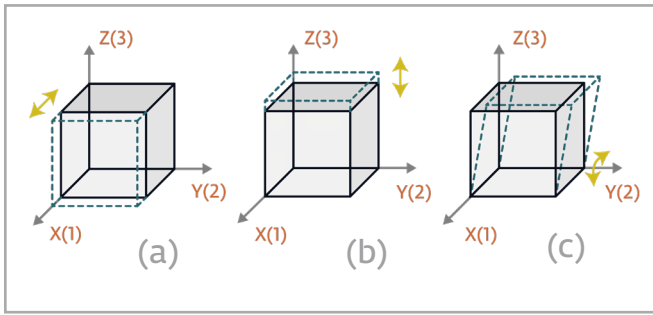


FIGURE 5: Different piezoelectric modes. (a) is d_{31} , (b) d_{33} and (c) d_{15} here rotating around Y axis (5). Adapted from unknown source.

subscript indicates which direction the strain is felt by the material. In this case d_{31} would be strained in a direction perpendicular to the poling direction, d_{33} would have the poling and strain vector parallel to each other. One last instance of this is when strain is applied in a twisting motion with the arrow rotating about the axis. The rotational directions are normally numbered 4 (X-axis), 5 (Y-axis) and 6 (Z-axis), like shown in figure 5c. The modes d_{31} and d_{33} are described in figure 5a and 5b, and electrode placement in figure 6.

2.3. Piezoelectric energy harvesters

The transducer ability of piezoelectric materials make them well suited for energy harvesting. Especially when it comes to harvesting of vibrational energy, the piezoelectric effect peaks in comparison to other methods. In comparison with other EH, the piezoelectric energy harvesters (PEH) are known for their low cost, easy implementation and variety of operating frequencies. Mostly they are known for producing high power density and are therefore considered the best available option when it comes to vibration based harvesters [9]. The properties of PEH are greatly decided by the material used.

Materials

There are several available materials with piezoelectric properties, and these can be set up in a broad variety of layers, shapes and configurations.

Piezoelectric materials are often categorized into crystallines, ceramics and polymerics [5, 8]. The material properties vary with factors like elasticity, power density, temperature range and coupling factor, and they should carefully be considered before choosing. The most commonly used

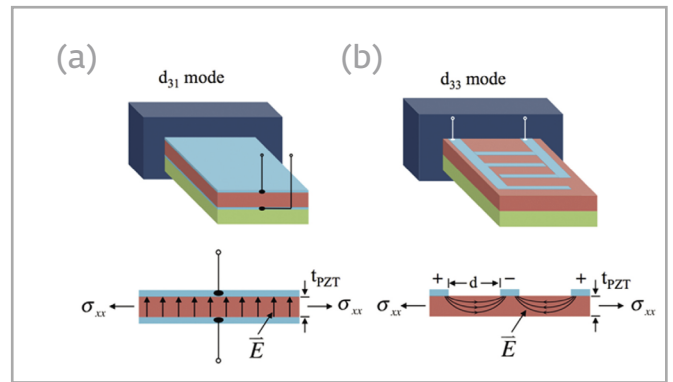


FIGURE 6: Electrode placements for mode 31 and 33. Source: Figure 8 (page 12) in [9].

are ceramics, like Lead Zirconate Titanates (PZT), but also other available materials, including Aluminum Nitride (AlN) and Zinc Oxide (ZnO). It is also worth mentioning Sodium Potassium Niobate (KNN), which is a promising lead-free alternative with similar properties to those of PZT materials.

PZT materials are considered as the top performing piezoelectric materials, and therefore they are the most frequently used. There are three common classifications of PZT, these are PZT-5A, PZT-5H, and PZT-5J [5, 8, 12]. For attaining wanted resonance frequency and energy output, the main difference between these three is the Young's modulus, quality factor and coupling coefficient, and also layer configuration.

Both 5A and 5J have a higher quality factor, which means that they have a narrower bandwidth, but higher output potential. 5H has a higher coupling coefficient than 5A, which is an important property for EHs [8]. 5H also has a lower Young's modulus than both 5A and 5J, which makes it more suited for vibration based harvesting. See table 3 for an overview of the properties.

Ability	Symbol	5H	5A	5J
Coupling	K_{31}	0.43	0.40	0.45
Density [kg/m ³]	ρ	7870	7950	7900
Q-factor	Q	30	80	80
Young's modulus *10 ¹⁰ [N/m ²]	Y_{11}	6.2	6.6	6.4

TABLE 3: Some properties for 5H, 5A, 5J [12] See appendix J for a complete list

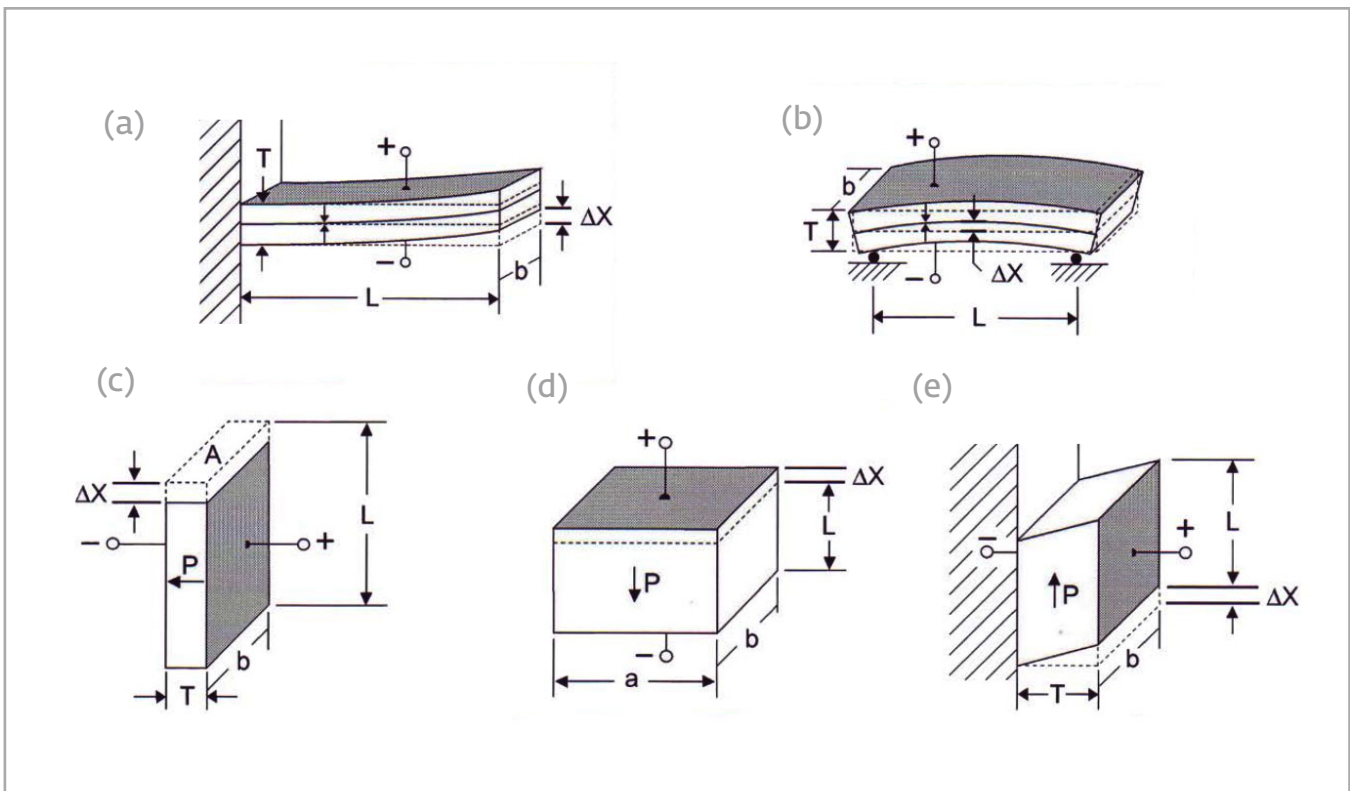


FIGURE 7: Common piezoelectric configuration: (a) Cantilever beam, (b) simply supported beam, (c) transverse, (d) longitudinal and (e) shear. Source: Table 3 (page 14) in [12]. See appendix K for related formulas and appendix I-J for properties and symbols.

It's not only the chosen piezoelectric material that determine the functionality of a PEH. The material of the protective layers, and the layer configuration also play a vital role. As so does the previously explained modes, as they demand different configurations.

Configurations

For layer configuration the two most common are unimorph and bimorph. Unimorph configuration has one layer of piezoelectric material, while bimorph has two. layers. Bimorph production is considered more difficult for use with micro electronics, thus most MEMS devices of today have a unimorph configuration [9].

Some commonly used configurations are; bending, compression, extension and shear. For bending generators, the main configurations are cantilever beam and supported beam (or supported disk). For compression, extension and shear, the specific configuration depends on the poling direction and where the force is applied. See figure 7 for an overview.

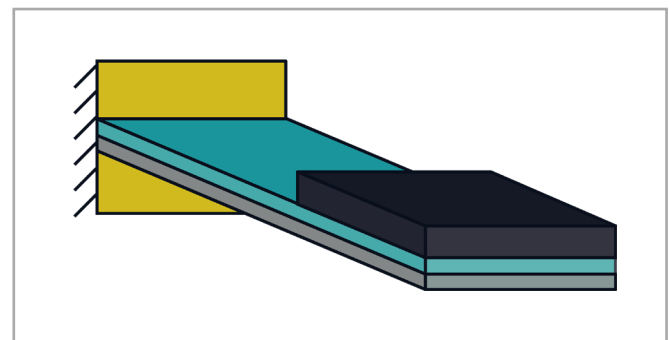


FIGURE 8: Cantilever configuration

Vibrations and resonance

Moving sources often result in vibrations, and when it comes to vibration based energy harvesters, there are some options more preferable than others.

Normally *vibration based EH (VEH)* are modelled as a *mass-spring-damper system (MSDS)* [9] (see section 3.3). The maximum power outtake is therefore dependant on acceleration, mass and damping, and is at its highest when the

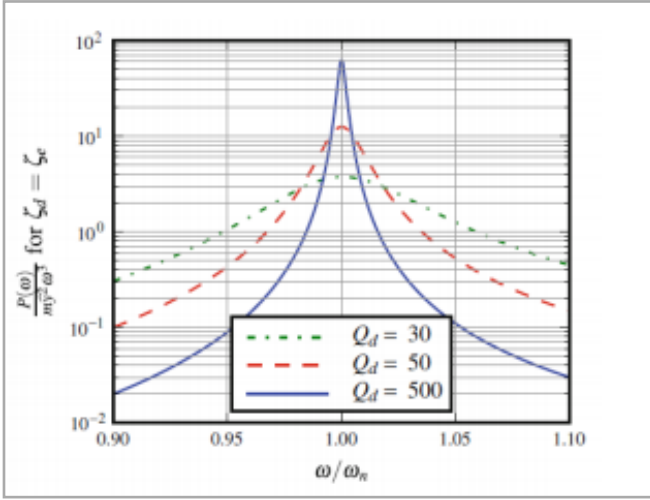


FIGURE 9: Q-factor and bandwidth. Source: Figure in [13].

resonance frequency of the harvester matches the natural frequency of the system (ω_n).

The relationship between resonance, acceleration (A) and deflection (x) are expressed by:

$$[4] \quad A = \omega_n^2 x$$

The amount of power one is able to draw from a PEH is highly dependent on the vibrating frequency. This means that efficient energy harvesters need to be calibrated such that they vibrate at their resonance frequency. This is called frequency tuning and is an important part of any well refined energy harvester. Depending on the piezo's weight, material and geometry the natural frequency of the harvester will vary greatly, so by changing a cantilevers parameters like; tip mass, length or clamping position, varying the stiffness or changing the tip mass' center of gravity, one will directly change the system's resonance [16].

The resonance can be calculated with:

$$[5] \quad \omega_n = \sqrt{\frac{k_{eff}}{m}}$$

Damping and bandwidth

Another aspect of frequency one must be aware of is the bandwidth. Most PEH have a relatively narrow bandwidth, which means that just a small deviation from the resonant frequency can greatly reduce the effectiveness of the PEH

[9]. The bandwidth of the system is closely related to the Q-factor. In some cases, the Q-factor is used instead of mechanical and electrical damping. The Q-factor is expressed by the formula: [13].

$$[6] \quad Q_m = \frac{1}{2\zeta_m}$$

$$[7] \quad Q_e = \frac{1}{2\zeta_e}$$

Where the damping ratio ζ shows the relationship between actual damping (B) and critical damping (B_C):

$$[8] \quad \zeta = \frac{B}{B_C}$$

And critical damping given by:

$$[9] \quad B_C = 2\sqrt{km}$$

The combined Q-factor can be expressed as the sum of these:

$$[10] \quad Q_{total} = Q_m + Q_e$$

Since the Q-factor and damping are reciprocal to each other, it is desired that the Q-factor is as high as possible. However, as the Q-factor increases the bandwidth decreases, so the trade off for a higher power output is a narrower frequency band given by:

$$[11] \quad BW = \frac{\omega_n}{Q}$$

Figure 9 shows how the Q-factor affects the sharpness and effectiveness of the EH. In almost every case, the Q-factor of commercially available PEH is found in the datasheet.

As already stated, the system is at its most efficient when the PEH matches the natural frequency of the surrounding system. Also the electrical damping ratio ζ_e should match the mechanical damping ratio ζ_m to achieve maximum power output. At a set acceleration, the power output is inversly proportional to the resonance:

$$[12] \quad P = \frac{\zeta_e}{4\omega_n(\zeta_e + \zeta_m)^2} m A^2$$

Furthermore, damping from the surroundings and the device design must also be taken into account. Assuming the operating environment inside the device is a viscous gas or fluid, and the PEH takes shape of a long rectangular

plate (l_r), the squeeze film air damping (B_{lr}) [14], can be calculated by:

$$[13] \quad B_{lr} = \frac{\mu W^3 L}{h^3}$$

Where W , h and L are the dimensions of the harvester and μ represents the viscosity of the surrounding fluid. It's worth mentioning that the viscosity of any gas or fluid is affected by both temperature and pressure.

Impedance matching

Another challenge when using PEH is the changing impedance, which varies from $k\Omega$ to $M\Omega$. It is therefore important to choose the correct resistance load. Since a real life animal won't produce a stable acceleration and frequency, it is important to match the output impedance of the harvester as closely as possible:

$$[14] \quad Z_{out} = Z_{load}$$

This is to achieve the maximum amount of transferred energy, and it becomes increasingly hard because of the dependence between impedance, acceleration and frequency.

The harvester's output impedance can be calculated by:

$$[15] \quad Z = \frac{1}{2\pi\omega C_p}$$

Where C_p is the piezoelectric capacitance and ω the vibrational frequency of the beam, here ω is not given as angular frequency, as seen in equation 21 on page 13 in [9].

The impedance and the resonance frequencies given by the datasheets are often an indicator of what to expect from the cantilever. That being said, this is usually dependent on the use case of the cantilever and testing environment. This means that the specifications of the datasheet should be somewhat questioned [15].

3. METHOD

The purpose of the literature review was to gain insight and further understanding of piezoelectricity and their transducer abilities. As this study contains a widespread of engineering disciplines it was crucial to establish an early baseline of understanding, and to account for challenges that usually fall outside the curriculum of a bachelor degree in instrumentation engineering.

3.1. Research

Literature study

To acquire a necessary foundation, the conduction of a thorough literature study was needed. Most papers were found in the commonly used database are *Oria*, which is accessed through *NTNU*. In addition, online publications such as *Science Direct*, *ResearchGate* and *Google Scholar* were also used. For searching, a number of keywords (see *table 4*) and boolean operators were used to help narrow down the results, and the abstract was read to determine the article's relevance.

Wanted word	Search words
Piezoelectricity	piezo*, crystal*, MEMS
Frequency	extremely low frequenc*, elf, resona*, vibrati*, oscillat*
Energy harvesting	energ*, harvest*, generat*, transduc*
Underwater	underwater, aqua*, sub*, marine, fish, animal
Movement	mov*, kinetic*, mechanic*, bend*, swim*, biomechanic*, tail beat*, in vivo
Modelling	simulat*, spice, Itspice, lumped, model*, tool*

TABLE 4: Search words and keywords

To get a foothold within the world of piezoelectric transducers, an online resource collection found on *Piezo.com* was used, as their compendium served as a good entry level on the topic [12]. Other online information hubs were also used, Mainly *Learnpiezo.com* and the Norwegian online encyclopedia "*Store Norske Leksikon*", but also through *Wikipedia* and sources found in their articles.

Seeing as the field of this paper is rather niche and the amount of research can be overwhelming, many articles were deemed irrelevant as their contents didn't address the specific questions at hand. Many relevant articles were also obtained through *Cuong Phu Le*, who was supervising this study.

Consultations

In order to gain the necessary knowledge of the biology, fish tagging and marine tracking, an interview with senior researcher *Robert Lennox* at *NORCE Norwegian Research Centre* was conducted, in addition to information obtained from *TB*. The questions asked aimed at understanding what specific set of challenges and considerations one should keep in mind when designing electronics that is to be placed in a living being.

Data collection

Two sets with live sensor data were acquired for this study, data set A, courtesy of *Martin Føre* (Associate Professor, Department of Engineering Cybernetics, *NTNU*) and data set B courtesy of *Jan Grimrud Davidsen* (Associate Professor/Research Professor, Department of Natural History, *NTNU*). In addition, the paper associated with data set A [17]. See *table 5* for parameters, and *appendix H* for example data.

	Data set A	Data set B*
Provider	Martin Føre	Jan Davidsen
Number of fish	3	1
Species	Atlantic Salmon	Sea Trout
Length	63-68 cm	49 cm
Weight	1-3 kg	740 g
Environment	Sea cages	Wild
Tag	DST + TB WSN	TB WSN
Sample frequency	20 Hz	NA*
Sample size	532379 per set	NA

TABLE 5: Parameters of data set A and B. *Data from three transmitters were given as data packages from three different receivers, no sampling frequency data.



FIGURE 10: Available transmitter sizes from TB [1]

3.2. Case

After consulting TB, a 1 kg *Atlantic salmon* (AS) was chosen as the case for this study. If the system provides an adequate power output, the possibility of downscaling will then be considered.

Data analysis

Before designing the EH, one must figure out the range of frequencies it will operate at. Since the harvester is located inside the fish it is natural to expect vibrations close to the frequencies of the fish's tail movement. The tail beat frequency varies with size and activity, and it was therefore decided to base both frequencies and acceleration on measurements from data set A. Accelerometer data in this set are represented by three values, one for each axis X, Y and Z. All three axes will have a gravity component depending on tilt and roll of the fish. The gravitational component was filtered out using a low-pass filter with a cutoff of 0.2 Hz. This cutoff is considered large enough to remove all trails of gravity, yet small enough to conserve any data of use, since frequencies below this cutoff are likely to have a negligible acceleration. After data filtering, the resultant vector of X, Y and Z are calculated according to [appendix G](#), and outputted to give an idea of the acceleration levels the harvest would get subjected to.

$$[16] \quad A_R = \sqrt{A_Z^2 + A_Y^2 + A_X^2}$$

$$[17] \quad A_{filtered} = A_R - A_{LP}$$

A *Fast Fourier Transform analysis (FFT)* was performed on the filtered resultant. The FFT is essential for revealing the most common frequencies of the fish's tailbeats, as it gives insight into the frequency components and the amount of power in each frequency bin. The resultant acceleration is then corrected and normalized to show the amount of power for each tailbeat component. The analysis indicated that most of activity lies around 1.5-2 Hz, which was expected. The activity increased during feeding, but still the acceleration found was usually between -0.1 to 0.1 G. However, according to Føre, there were instances where the movement would fluctuate, reaching accelerations up to 2 Gs in short bursts [17].

Data set B contains the RMS acceleration from the Sea Trout, but because of the lack of uniform transmissions, it was not suited for the FFT algorithm, making the tail beat frequencies hard to obtain. Instead, the data was imported to MATLAB, where the max and average acceleration was extracted.

Expected operational area for EH

Frequency range [Hz]	1–3
Acceleration (average) [G]	0.1

TABLE 6: Frequency and acceleration area. Based on data set.

Requirements

For the EH to be sustainable, the power outtake needs to match the power consumption of the WSN, or at least a certain amount of it to justify the implementation. Further, the energy needs to be converted from AC to DC, and stored with minimal loss.

Power requirements

Current requirement [μ A]	5.0–10
Driving voltage [V]	3.3–4.0

TABLE 7: Current and voltage requirements for WSN

It's a reasonable estimation that an individual AS of 1 kg has a length of about 50 cm, this was confirmed by TB. They also stated that the maximum length of the system should not exceed 20% of the fish's total length, and that the weight should not exceed 2%. This was also supported by Lennox.

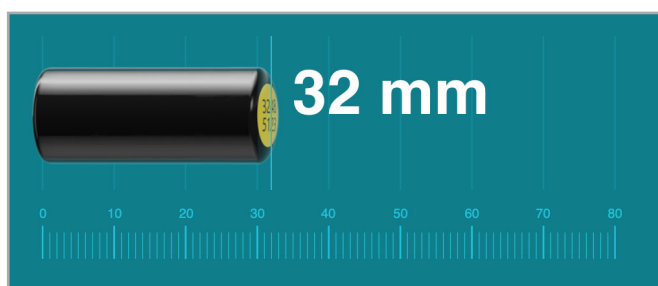


FIGURE 11: Size of chosen transmitter

This leaves a total of 100 mm and 20 g for the combined system of both WSN and EH module. TB's transmitters span across a large range of marine species, and the WSN varies in both size, weight and lifespan.

The chosen transmitter series is therefore decided to be in the 13 mm range, with a length between 27.9 and 38.7 mm and a weight between 9.19 and 13.8 g. See *appendix E* for an overview. The decided size and weight requirements are listed in *table 8*, and estimated battery life of the transmitters is listed in *appendix F*.

	Weight [g]	Length [mm]	Diameter [mm]
Case (AS)	1.00 k	500	NA
System	20.0	100	12.7
WSN	9.19–13.8*	27.9–38.7	12.7
PEH	10.0	70.0	12.7

TABLE 8: Geometrical parameters for the individual parts of the sensor system (both the WSN and the PEH module). * weight in air.

Disclaimer: It's worth mentioning that the requirements are set to work as a base. For the purpose of testing in a limited time frame, small deviations are therefore allowed. Also, the overall goal of the EH module is to reduce the need for batteries, which, according to TB represents the main weight of the WSN. Because of the reduction in battery weight, the added module may also decrease the overall weight of the system.

Chosen configuration

Bending generators are most interesting for the purpose of bending or vibrating with movement. There were two solutions considered for this assignment.

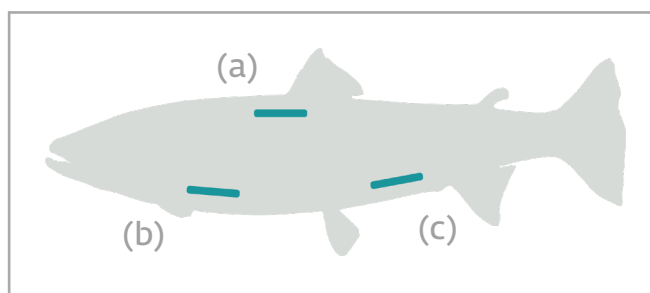


FIGURE 12: Placements of implanted beam. (a) along the dorsal fin, (b) abdominal cavity, or (c) Near the tail fin.

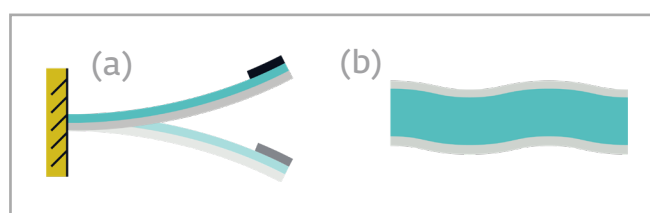


FIGURE 13: (a) cantilever configuration, and (b) film beam configuration.

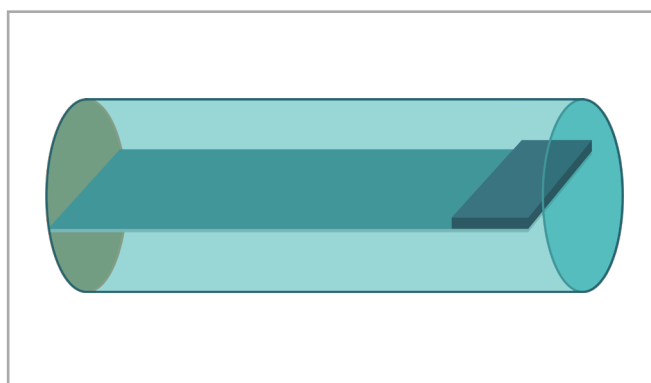


FIGURE 14: Cantilever inside gas filled container.

Solution A, film beam: The beam can be placed both internally (implanted) or externally. If implanted, the beam will get excitations from bending as the fish moves. If placed externally, the beam will get excitation from both fluid flow and swimming motion.

Solution B, cantilever beam: With this solution the beam inherits vibrations from the tail beat frequency. To get a sufficient output, the natural frequency of the beam needs to match that of the fish in order to get the correct resonance.

For both internal and external placement, the beam would ideally be placed either near the tail fin or along the dorsal fin, but the abdominal cavity is the preferred solution (see *figure 12*).

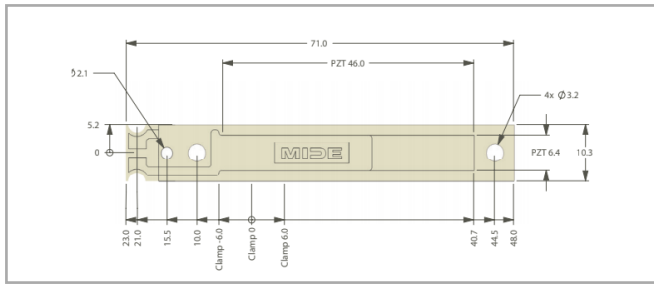


FIGURE 15: Chosen harvester, S129-H5FR-1803YB [22]

Both TB and Lennox agreed that a protected module placed in the abdominal cavity was preferable for both WSN and EH. Therefore solution B was chosen for this study.

Chosen harvester

The best available harvester option was the Midè S129-H5FR-1803YB (PPA-1020). See appendix L for properties. The harvester has a resonance of 49 Hz. In some cases this might be considered as low frequency, however far from the desired 2 Hz range, which is optimal for the purpose of this study. It was therefore decided to order two specimen, for the purpose of modifying one. This is explained further in section 5.1 and 5.4.

3.3. Simulation

Modelling

Two systems can be said to be analogous if they are physically different, but have a set of corresponding differential equations. In the case of the MSDS and the RLC circuit, these conditions are met by the system's obvious physical differences and the following differential equations.

First we will look at the MSDS:

$$[18] \quad F = m\ddot{x} + B\dot{x} + kx$$

$$[19] \quad F = m \frac{d^2}{dt^2} x + B \frac{d}{dt} x + kx$$

Where F is the sum of all forces acting on the system, m is the system's inertial mass (in this case the proof mass), B is the damping coefficient and k is the stiffness.

As for the circuits, we use Kirchhoff's law of potential difference to derive the equation:

$$[20] \quad V = L \frac{d}{dt} i + Ri + C^{-1} \int_0^t i dt$$

By substituting the current (i) with the following:

$$[21] \quad i = \frac{d}{dt} q$$

Where q is the charge (in Coulombs) we get the following formula:

$$[22] \quad V = L \frac{d^2}{dt^2} q + R \frac{d}{dt} q + C^{-1} q$$

Where V is the circuits electric potential, R is the resistive load, L is the inductance and C is the capacitance.

If we compare eq. 18 and eq. 22, one will recognize that both equations have corresponding terms, each of the terms has a matching correspondent, and because of the nature of differential equations we can expect that the RLC- circuit will act as a MSDS. Now it is just a matter of finding the coefficients for the components that best represent the system.

Analogies

Domain	Domain
F	V
\dot{x}	i
m	L
B	R
k	C

TABLE 9: Analogies for the e→v model

Force (F) to Voltage (V): The sum of all forces acting on the system represented as the total difference in electrical potential.

Velocity (\dot{x}) to Current (i): The current running through the circuit is analogous to the velocity of the mass.

Inertial Mass (M) to Inductance (L): The inertia of a mass will resist change in velocity the same way an inductor resists the change in current.

Damping (B) to Resistance (R): The mechanical energy will dissipate as heat or sound. The electric energy will, likewise, dissipate as heat through a resistor.

Spring Constant (k) to Capacitance (C): A spring that oscillates between its critical displacement is analogous to how a capacitor is polarized [ch. 5 in 18].

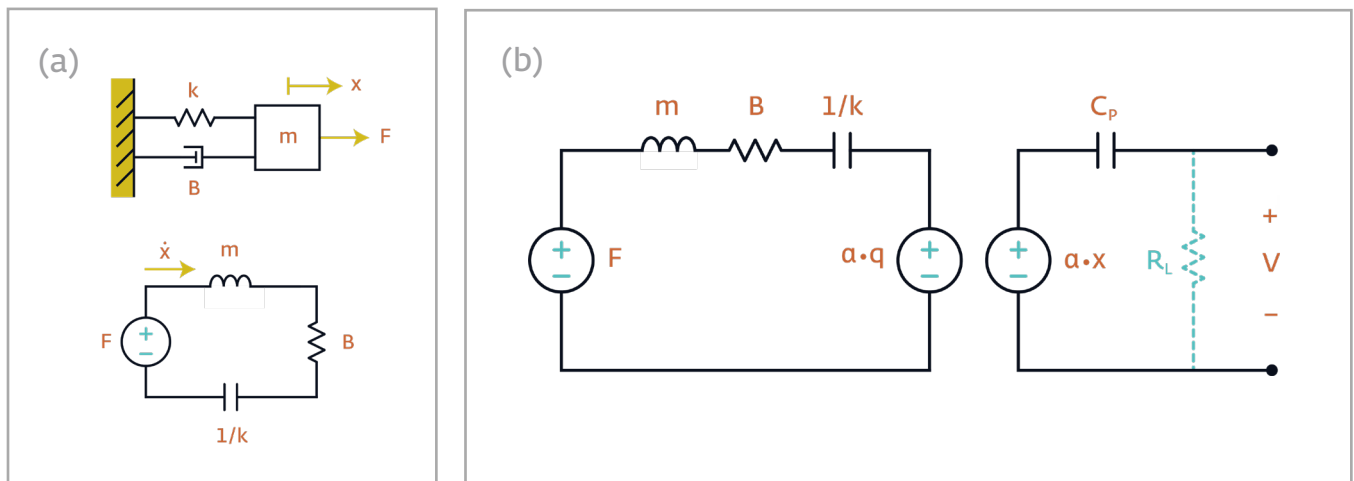


FIGURE 16: Mechanical to electrical analogies (a) MSDS to electric conversion and (b) Equivalent circuit diagram.

Simulation setup

All parameters used in the simulation, except the stiffness are gathered from the datasheet of the harvester. The stiffness of the cantilever was calculated after testing various frequencies and proof masses, using the following equation. we can derive the cantilevers stiffness:

$$[23] \quad k_{eff} = m\omega_n^2$$

MATLAB was used to generate a chirp signal, (see *appendix P*). This signal was then used in the simulation to perform a frequency sweep. When used in the simulated circuit, see *appendix N* for circuit in LTspice, the output of the simulation will display a huge gain in voltage when the frequency of the sweep is closing in on the system's resonance.

With all parametr gathered and the case decided upon, simulations were initiated. Measurements gathered were outtake voltage and current over a set load resistance.

Parameter	Value
C_p [nF]	22
k [N/m]	149.5
K	0.44
R_L [k Ω]	300
m [g]	10
B [Ns/m]	0.02
A [G]	0.1

TABLE 10: Simulation parameters

3.4. Test rig

For testing of the PEH, a reliable and stable system is needed. This system must also be such that it can replicate some of the motion found inside the fish. Since recreating an environment that can replicate the abdominal cavity is not feasible, given the time restrictions, it falls outside of this paper's scope.

Setup

The setup is made up of: shaker, function generator, oscilloscope, multimeter and an amplifier. Although this is not sufficient to replicate the right conditions it is capable of proving the principles of frequency tuning. For full list of instruments and components, see *appendix A*.

The shaker was used to replicate the sinusoidal movement of a fish's body. A beam was screwed to the shaker and the piezoelectric cantilever was fastened with a screw, between the clamping plates. A proof mass was fastened with self-adhesive tape to the free tip of the cantilever. It is worth mentioning that the geometry of the masses used was not ideal.

To measure the acceleration of the system an accelerometer was added to the base of the cantilever. The cantilever was probed and measured with the oscilloscope and multimeter. The shaker was powered by a function generator and an amplifier. To not damage the shaker the source was limited to $3 V_{RMS}$. Resonance tuning was performed by changing the weight of the proof mass. Lastly, the voltage was measured over a potentiometer to find the maximum transfer of power generated by the EH.

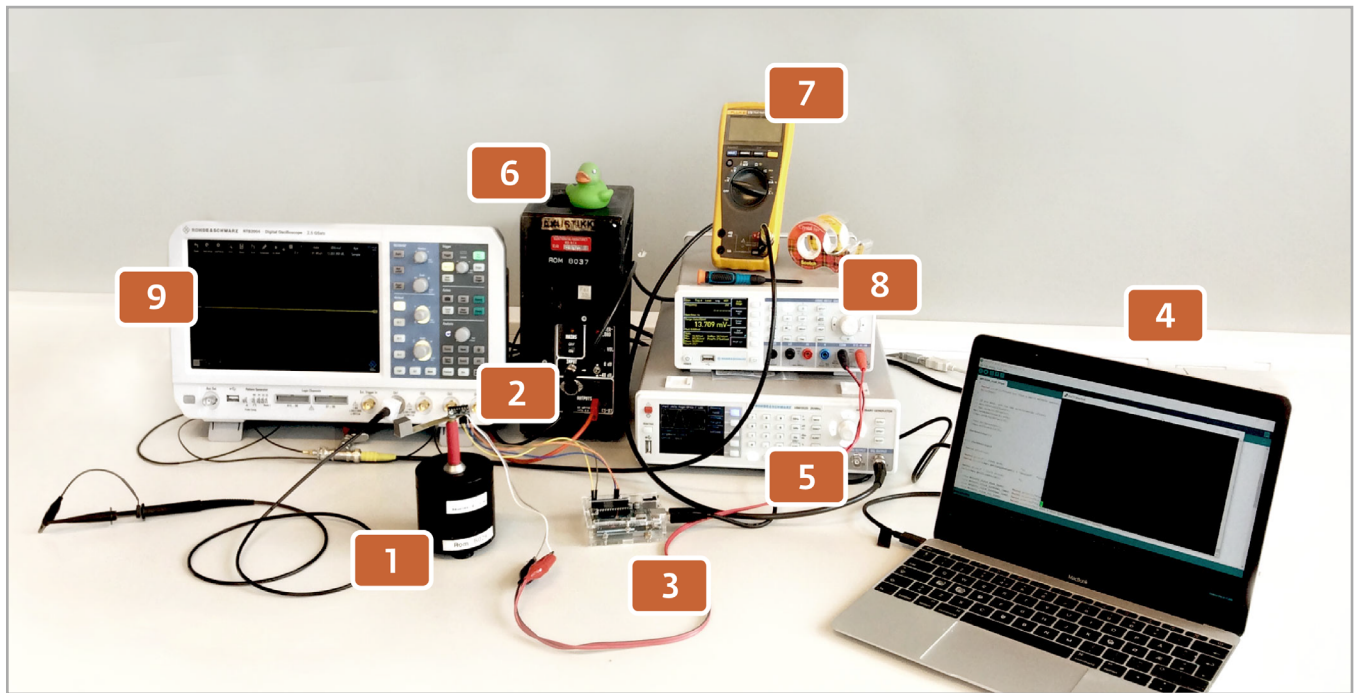


FIGURE 17: Setup of test rig

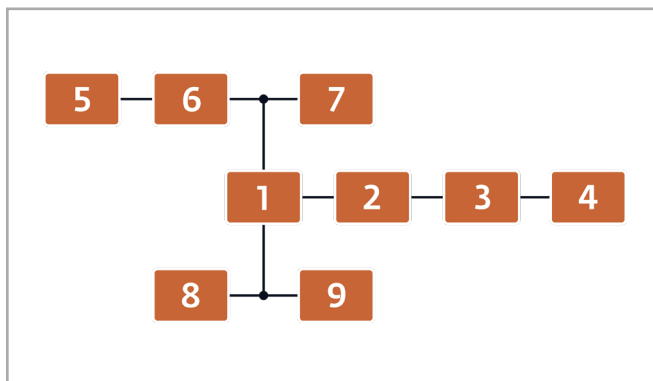


FIGURE 18: Block diagram of setup

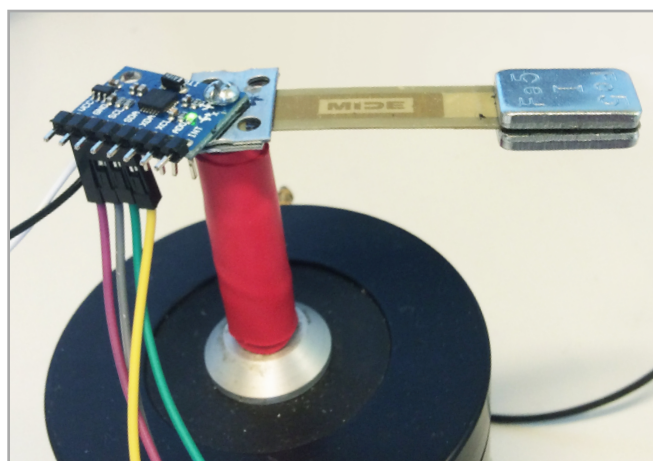


FIGURE 19: Cantilever B with proof mass.

Instruments in setup

1. Shaker
2. Accelerometer
3. Arduino Uno
4. PC
5. Function generator
6. Amplifier
7. Multimeter (for shaker monitoring)
8. Multimeter
9. Oscilloscope

Accelerometer configuration

The accelerometer chosen is the *MPU 6050*. This accelerometer uses I2C communication, and therefore needed to be connected to a microcontroller. Due to the complexity of the I2C protocol and the limited time, it was decided to use an existing library licensed through GNU GPL, for initialization, and further use *Arduino UNO (ATmega 328p)* [21] as the controller and *Arduino IDE* for the output coding. This library contains ready-to-use functionality.

The acceleration output code (*appendix U*) was then set up from an example code, and edited to adjust for gravitational force. Furthermore, the absolute values was used to calculate average acceleration (from a statistics library). Both libraries are listed in *appendix C*. The output from PuTTY can

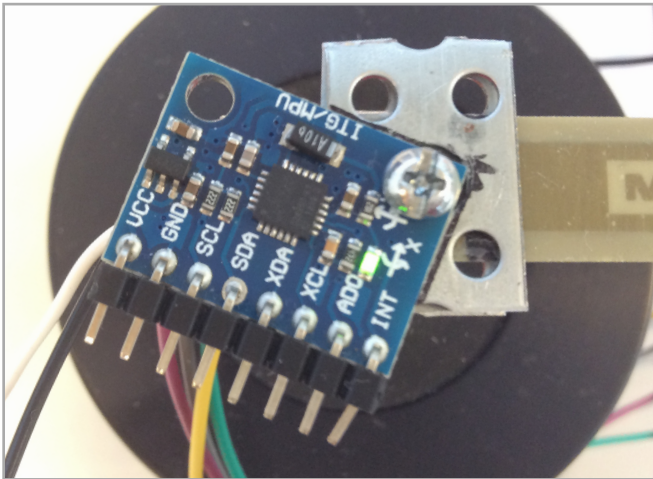


FIGURE 20: Accelerometer installed at the base of the shaker

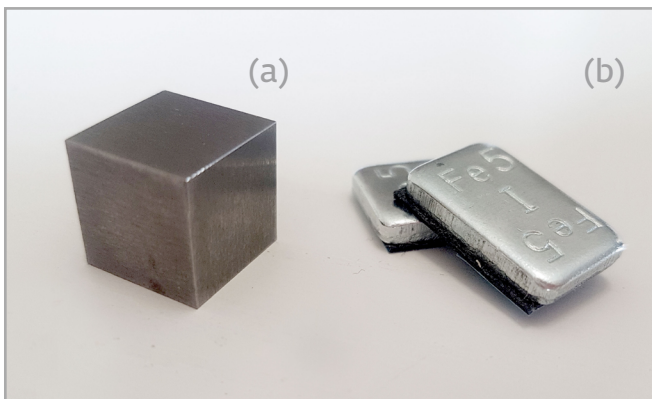


FIGURE 21: Proof mass used. (a) tungsten weight, 37.25 g. (b) Iron weights, 5 g.

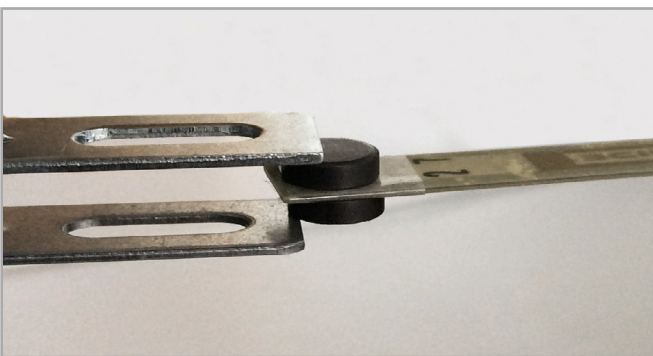


FIGURE 22: End stop and magnets on cantilever A.

be seen in *appendix V*. Since the accelerometer measures in three directions, and the shaker is one dimensional in its movement, the output only contains information from the Z axis to represent the resultant acceleration from the data sets. Measuring all three axes would not be possible with the setup. Also the only available data with acceleration components from all three axes, is set A from Martin Føre [17]. Set B from Jan Davidson (*appendix H-2*) only provides the resultant acceleration vector, and not the individual components. See *section 5.4* for a discussion on the uncertainties this produces.

Frequency tuning

As mentioned in *section 2.3* the most feasible way of obtaining the desired resonance is to change the proof mass and/or the geometry of the cantilever itself. This is because the other properties, such as stiffness and damping are material properties, and are hard to change.

According to the datasheet the cantilevers have an effective stiffness of 261.21 N/m, when fastened at clamped at position: 0, with no tip mass. The resonance was lowered by adding weight to the tip of the cantilever. To further lower the resonance the clamp position was moved to position -6 (see *appendix L-1*).

The last option for lowering the resonance was to reduce the stiffness of the cantilever was changing its geometrical shape. To do this, one of the cantilevers was thinned down to a thinner profile from 0.76 mm to 0.6 mm, which will hereby be referred to as Cantilever A and Cantilever B, respectively. Both cantilevers were, in turn, strapped to the shaker and exposed to increasing levels of accelerations.

3.5. Experiments

To test the effect of non-linearities, an experimental rig was set up. This included two endstops and a proof mass in the form of two magnets, as shown in *figure 22*. The results are presented in *section 4.4*, and will be discussed further in *section 5.5*.

4. RESULTS

This section shows the spectrum analysis from preparational work, in addition to results from both simulation and measurements from the test rig. All MATLAB codes are presented in *appendix O-T*.

4.1. Preparations

Activity data

The data from the accelerometer (data set A) used in the series of tests performed by [17] were processed and analyzed using MATLAB and the FFT function (see *appendix O*).

The results of the analysis shows that, normally the activity of the sensor is measured around 0.1 Gs and between 1 to 2 Hz. That being said, there are visibly components of higher acceleration present on the spectrum. The figure below depicts the activity level of one of three tagged salmon from the enclosure. The fish is observed being mostly calm, with a few exceptions where small spikes appear. Largest are the spikes at the start and end of the time-series. The spikes are most likely captured during feeding. These outliers will be addresses later in the discussion section of this paper. There were also observations by Føre [17] showing sudden bursts of acceleration in shorter moments. Seeing as the acceleration exceeds the 0.1 Gs mark in the 1-2 Hz range a conscious decision was made to conduct the measurements at an average rate 0.1 Gs. The reason being that this would put us in the 0.1 to 0.15 Gs range as shown in *figure 23*. The values from data set B shows that the Sea Trout average recorded activity was at 0.026 G, with a peak acceleration of 0.195 G.

Modifications

The testing of the EH was performed on two cantilevers of the Mide S129 series. Both cantilevers were tested with the same weight of 10 grams and a base acceleration of 0.1 Gs. This test revealed that the stiffness of an unmodified cantilever was closer to 249.5 N/m, when fastened at clamp position -6, and had a resonance around 24–25 Hz. Testing the modified

cantilever revealed a stiffness of 149.5 N/m. which brought the resonance down to around 19 Hz. This indicates the relationship between the stiffness of the material and the resonance, proving that for extremely low frequencies a much softer material is preferred for harvesting vibrating or bending energy.

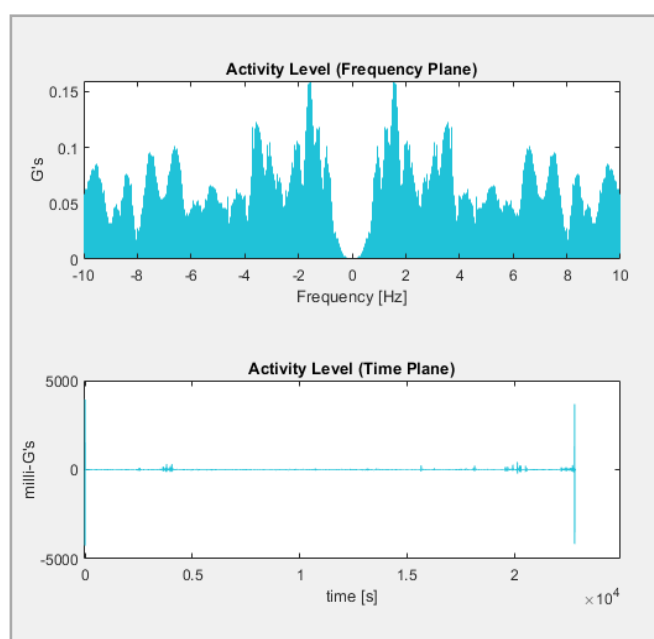


FIGURE 23: Spectrum analysis of data set A

The cantilever was thinned down from 0.76 mm to about 0.6 mm across the whole active area of the cantilever. To further reduce the resonance increasing weight of 15, 20, 30 and 37.25 g is fastened to the cantilever.

4.2. Simulation

The results from the simulation are split into two parts; one part to show the system's response to a chirp signal and one to show the output at an operating resonance frequency.

Frequency sweep

Figure 24 shows the response to a simulated frequency sweep (chirp). The sines amplitude is representative of the

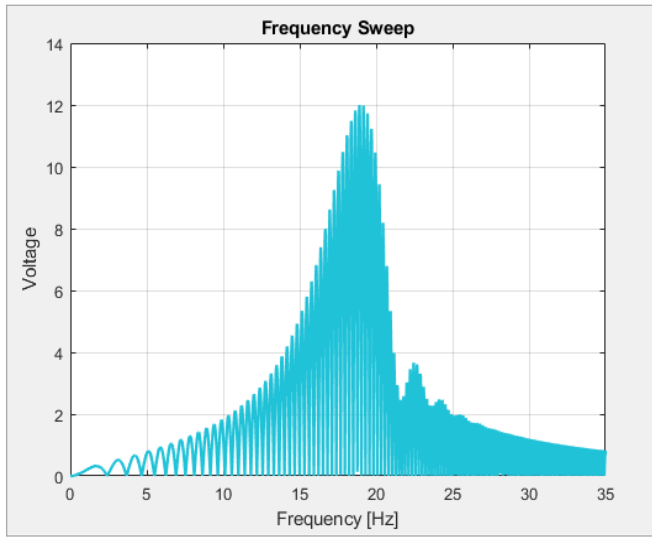


FIGURE 24: Frequency sweep from simulation.

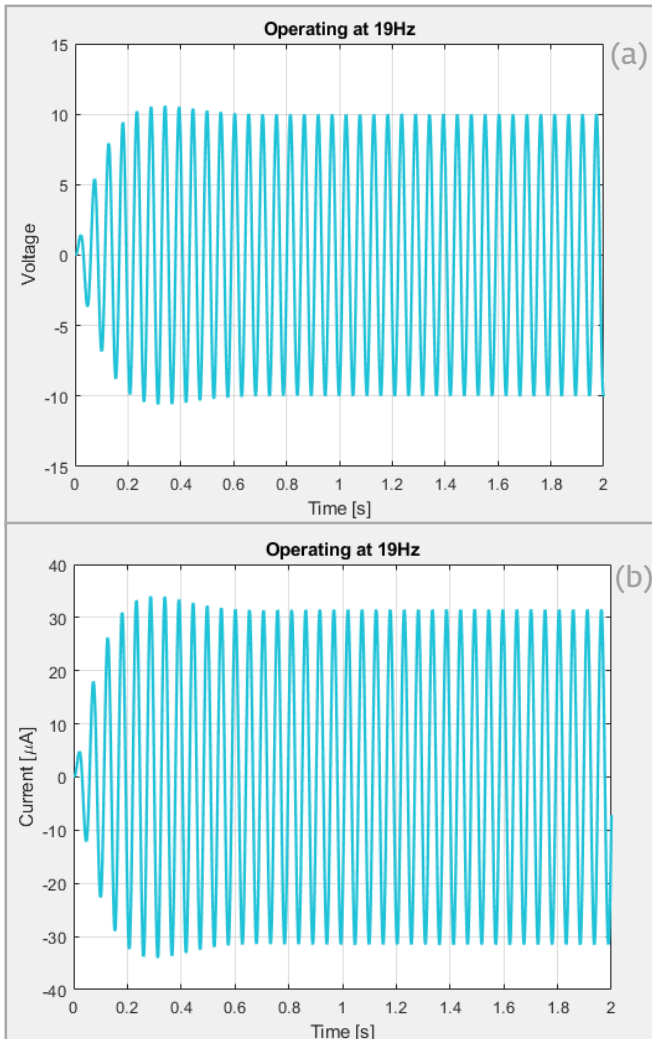


FIGURE 25: Simulation circuit operating at resonance: (a) generated voltage. (b) generated current.

EH voltage output over a 300 kΩ resistor and the input force is 0.1 Gs. The peak is just short of 19 Hz.

Operating at resonance

In [figure 25a](#), the graph shows the voltage output of cantilever B operating at its resonance frequency of 19 Hz with a stimulus of 0.1 Gs.

4.3. Test rig

The main challenge is to tune the PEH to a frequency as close to the tail beat frequency as possible and still stay within the boundaries for the given case. The tests made it clear that the more the piezoelectric material is displaced the more voltage and power is generated. In addition to this, the internal resistance of the cantilever appears to also decrease as the bending increases. This is the trend for both cantilevers although their output was not the same.

Frequency sweep

Both measurements show a similar behavior, with a spike around their resonance frequencies and small spikes in the lower frequency ranges which seem to have been shifted in parallel. See [figure 26](#). For the purpose of finding resonance frequencies for different proof masses, a series of tests were performed on both cantilevers. See [table 11](#).

Operating at resonance

Measurements over different loads were completed to investigate the degree to which the EH could transfer power. For this the terminals of the EH were connected to a potentiometer with signal frequency of 19 Hz with an average acceleration of 0.1 Gs (from the base of the shaker).

The optimal load for maximum power transfer, which is shown in [figure 28a](#), was calculated by multiplying the voltage and current from [figure 27](#) according to:

$$[24] \quad P = UI$$

The system was able to deliver almost 4 V_{RMS} and 15 μA_{RMS}. The power produced with these values comes to almost 60 μW. Measurements of differing accelerations were also tested for different loads. The result it shown in [figure 28b](#).

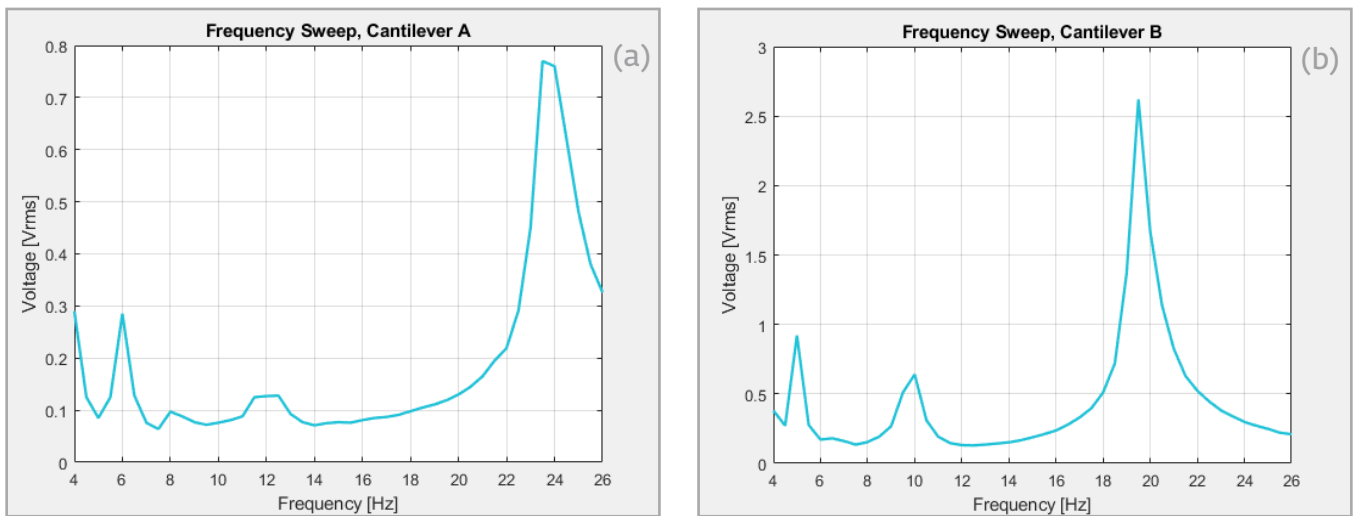


FIGURE 26: Frequency sweep from test rig: (a) Unmodified cantilever A with a stiffness of 249. (b) is the modified cantilever B with a stiffness of 149.5.

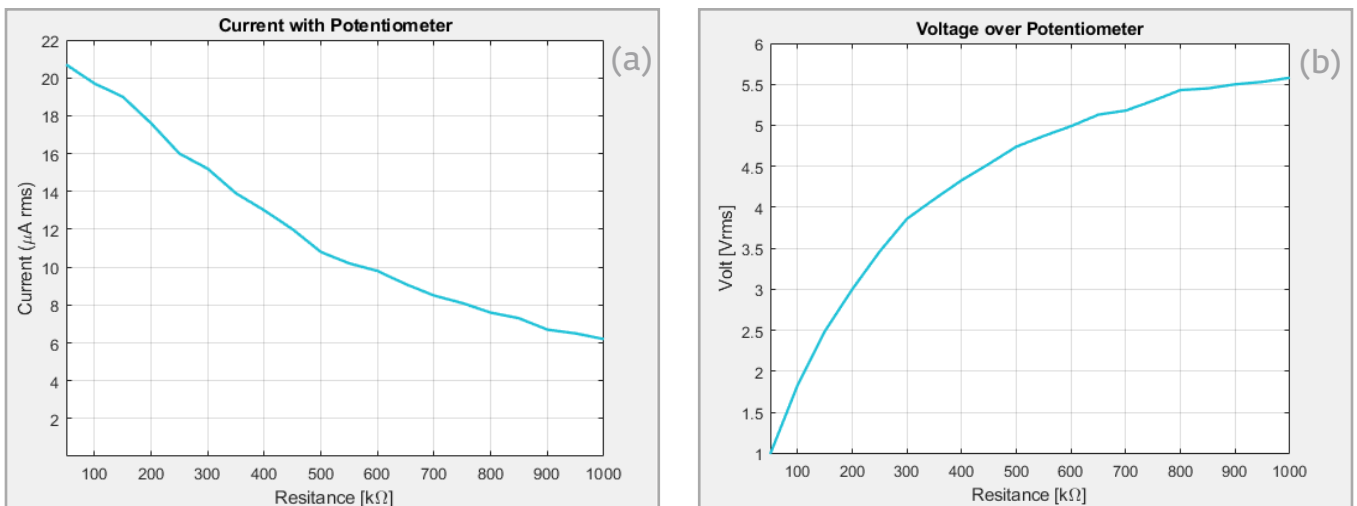


FIGURE 27: Test rig measurements over potentiometer: (a) voltage, and (b) current.

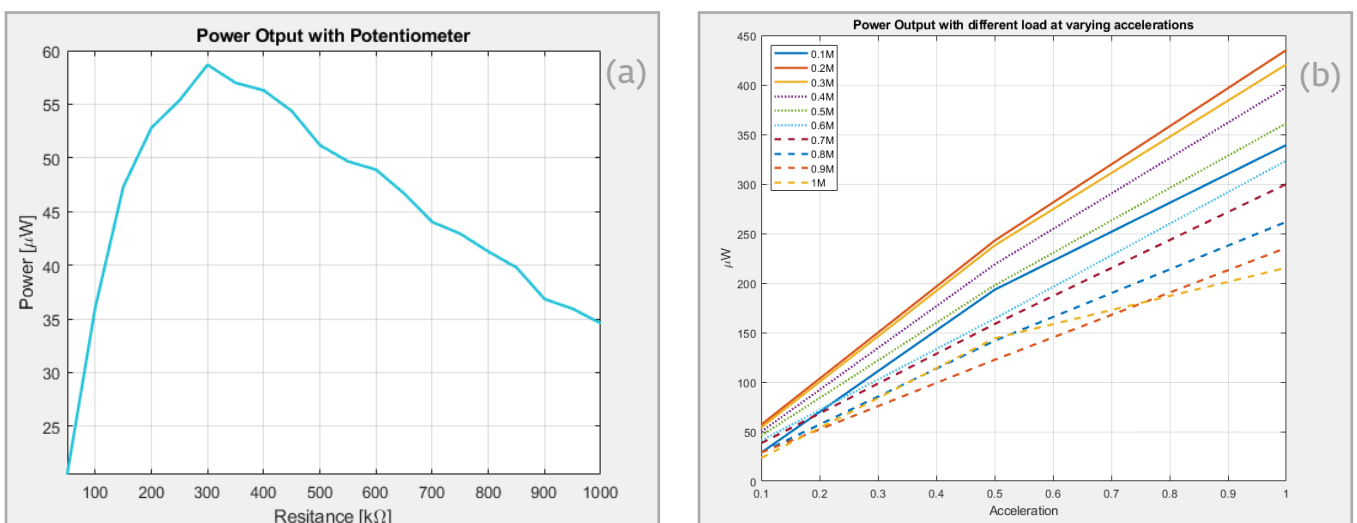


FIGURE 28: Power measurements: (a) Power from test rig. (b) Measured power with changing load at different accelerations.

	Proof mass	Resonance	Voltage	Impedance (out)	Current
	[g]	[Hz]	[V _{RMS}]	[Ω]	[μA _{RMS}]
Cantilever A	5	35.5	0.8	inf	0
	10	25.14	0.85	inf	0
	20	17.8	2.4	56 M	8
	30	14.5	3.36	45 M	8.7
	37.25	11.7	14.2	130 k	36.5
Cantilever B	5	26.87	1	inf	3.8
	10	19	2	74 M	7
	20	13.4	4.45	3.5 M	10.6
	30	10.96	4.4	3.5 M	9
	37.25	8.15	11	205 k	21

TABLE 11: All measurements were taken with an peak acceleration of 0.1 G.

4.4. Experiments

Results from the experiments are only included to show tendencies. Table 12 shows the values and figure 29 shows an oscilloscope screen capture of the measurement with the weaker magnet. Peak 1 at 4.9 V is when the magnet loses hold of the endstop, while peak 2 is when the piezoelectric beam deflects and hits the endstop on the other side. See section 5.5 for a discussion around the findings.

Configuration	2 x endstop 2 x magnet	2 x endstop 2 x magnet*
Frequency [Hz]	2	2
Base deflection [mm]	4	4
Height of mass [mm]	7.5	7.5
Height of gap [mm]	8	8
Peak 1/2 [V]	5.5/2	4.9/2.5

TABLE 12: Results from initial tests *weaker magnet

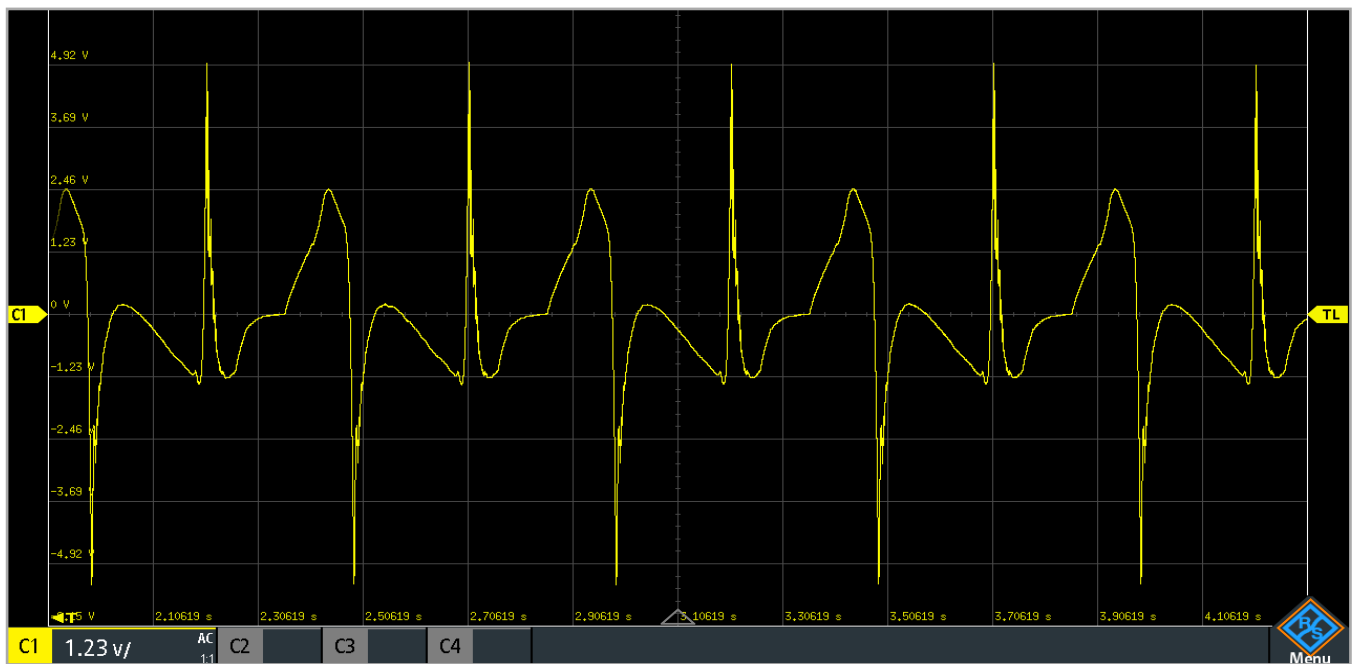


FIGURE 29: Endstop and magnet experiment, measurement from oscilloscope

5. DISCUSSION

The purpose of this study is to investigate the possibilities of successfully harvesting kinetic energy from the AS to power TB's WSN. Early in the process the decision was made to focus on the use of a vibrating cantilever. The reasoning for this decision was that it would be less damaging to the animal and the means of testing the output of a vibrating cantilever was easier to accomplish with more readily available equipment. To simulate the movement of the fish the cantilever was fastened to a shaker. As the container is placed inside the AS, the oscillations would propagate in the cantilever.

5.1. About the case

As mentioned in *section 3.2*, a cantilever inside a gas filled container (solution B), was chosen over a bending film beam (solution A). The placement of the container was set to the abdominal cavity. Solution B with abdominal placement is considered the least invasive for the fish, as an object placed in adipose tissue, in time, will be encapsulated.

Regarding solution A, an exterior beam placement was one of the earlier alternatives, but since this would demand penetrating the skin with wires, it was scrapped at an early stage. Penetrating the fish's skin would make it prone to infections and degrade its overall health. An externally placed device would in addition also make the fish more visible to predators and it increases the risk of getting stuck, which again could cause tearing and damage to the body. Two other solutions were considered for interior placement, either along the dorsal fin or close to the tail fin.

For placement alongside the dorsal fin, Li et al. [6] proved that it is possible to get an adequate power output from a rainbow trout, which has similar anatomy to that of a AS. But placement of a beam directly in the tissue is more damaging for the fish, and especially close to the spine, as it will affect the range of movement. Also this would put extra strain on the beam, making it more susceptible to breakage.

The cantilever beam inherits low frequency vibrations from the fish, and to achieve the maximum energy output it

is utterly important to get the frequency tuning right. As explained earlier this is done by lowering the resonance frequency, which is affected by two parameters, stiffness and added weight.

Stiffness and resonance

As shown in *section 4.3*, the resonance configuration by changing the proof mass on the tip of the cantilever, resulted in a lower frequency. This process is very simple, but what it also does is change the center of gravity which also affects the system's resonance. Changing geometry of the cantilever can be done by altering clamp-position, width, thickness and shape.

One solution might be to get a more customized produced piezoelectric cantilever, where the stiffness of the beam is reduced from the production side. One can choose a narrower beam, thinner protection layers or using protection material with more elasticity than FR4,

As an experimental test, the bottom FR4 layer on beam B was sanded down, to see how much stiffness reduction it was possible to attain. As the results show, by thinning down the cantilever from 0.76 mm to 0.6mm we were able to reduce the resonance by 24%, while this is a good starting point, it is not enough to obtain an effective EH at the 2 Hz range.

Proof mass

The main solution for the proof mass configuration became attaching one 5 g iron (Fe) weight to each side of the cantilever. The iron weights used for this were balancing weights used for car tires and they were bought locally at Biltema in Trondheim.

The stiffness is inherited by the material properties and layer configurations, and is difficult to alter once the beam is produced. So to attain a frequency between 1 and 3 Hz, with the original stiffness of beam A, the proof mass has to be around 1 kg. This is obviously not a possible solution, since 1 kg also is the weight of the AS case. Furthermore,

with a weight that high, the cantilever beam will not be able to vibrate. And finally, to really emphasize why this is not a suitable solution, the material with highest density is Osmium, and 1 kg of Osmium is approximately 44 cm³ [23] that is to be fitted inside a 10 cm long container with a diameter of 12 mm.

This presents the question of maximum displacement of the tip of the cantilever. For the testing purposes two iron balancing weights were used as proof mass, one fastened to both sides of the cantilever. As mentioned in *section 3.4*, the proof mass used was not ideal. The mass added a height of 3.0 mm each, making the total height of the cantilever's tip mass approximately 6.8 mm in total. At an average acceleration of 0.1 Gs the peak to peak swing of the proof mass is 13.5 mm, which is 0.8 mm greater than the diameter of the container. However, using a denser proof mass (like the commonly used Tungsten), would reduce the volume, giving it more room to move around.

It is necessary to investigate other methods of tuning. See *section 5.7* for a discussion on this

The chosen harvester

It is clear that the system tested in this study has its limitations when it comes to lower frequencies and the power said frequencies allow it to produce. The Midè S129 would work very well under other conditions, like harvesting vibrational energy from industrial motors or other forms of vibrating machinery. The assessment of the tests is that a more suitable approach to the problem would be to focus on the energy produced by bending of the PEH like showcased in [6], as opposed to strictly vibrations.

5.2. Activity data

Limitations of data

There were limitations in the number of available data sets, with information that accurately describes the chosen case. Data set A was exclusively from caged AS, whilst data set B was from an Ocean Trout. Preferably the data would be from individuals closer to our chosen case, but it is assumed to be close enough. If anything the level of activity of the caged AS is lower than that of the wild AS.

The reason for choosing data set A over B, was based on the fact that it was a continuous set of values, taken over

a longer period. It was therefore well suited for an FFT-analysis. The data in set B, on the other hand, is sampled and transmitted in larger sample packages, with gaps between reception. The data from data set B could offer an average level of activity, as well as the maximum recorded acceleration.

Placement

It is also important to note that the placement of the logger in data set A was on the AS' dorsal fin. The accelerations may therefore be different from what the chosen case has proposed. Because of this difference in placement, some uncertainties are expected. The data from data set B, on the other hand, is from an implanted WSN inside a Sea Trout. This data shows a lower level of activity than data set A. However, it is from another species than the AS.

5.3. Simulation

The overall system, including WSN, PEH and the fish is a multi physical system with various degrees of freedom which are difficult to account for. Because of this, many of the parameters are based on presumptions and approximations. Consequently the designed system contains simplifications that may not take into account all the necessary parameters for accurate results. Without heavy simulation based on precise mathematical models of all subsystems, the model used is susceptible to uncertainties and deviations.

Model limitations

The parameters one can alter are limited by the chosen simulation program and model. It is of course possible to add parameters like roll and tilt in LTspice, but after consulting with our supervisor, it was decided to only look at the resultant acceleration vector. Three vector components would be difficult to transfer to the one-dimensional test rig. Furthermore, only data set A contains individual components, as data set B outputs the resultant acceleration.

Another limitation in the simulation is that the acceleration amplitude in LTspice uses peak values, while the real measurements use average values based on acceleration data..

If one were to include parameters like temperature and pressure, a finite element model would be advised, using COMSOL or similar multi physical programs.

Either way, both temperature and pressure were here considered negligible for the operational range of the PEH.

The most complex parameter to calculate is damping. Damping relies on many variables, and there are too many factors to calculate a precise value. The cantilever is inside a gas filled container which then again is located inside a living being. The damping is affected by the adipose tissue, propagation of the tail vibrations, viscosity of the gas (air damping), material properties, temperature, pressure and the orientation of the fish (and therefore also the orientation of the cantilever).

Simulation verification

As mentioned in *section 3*, the method of simulating the PEH is with use of the analogous MSDS, RLC circuit. The way the simulation was verified was by recreating the circuit shown by Blystad et al. [24]. Once the circuit could recreate the results from the article it was considered ready for use. It was discovered that the circuit used in simulations was a sufficient method of investigating the resonance frequency for the cantilever. However there were some factors like mechanical damping and air resistance that would result in small deviations between measurements and simulations. These factors are hard to estimate and needs testing to make more accurate approximations. Because of this, the accurate damping coefficient is not included for the setup.

Deviations

There are obvious deviations between the simulation and the real results from the test rig. As discussed in the previous paragraph, the change in thickness of cantilever B will bring a level of doubt in respect to the effective stiffness of the cantilever. The only way to require some notion of what the stiffness was at this point was to conduct tests. Using the shaker to adjust the frequency to the cantilever's resonance was the most feasible way of approaching the problem. There are also other uncertainties that would affect the accuracy of the simulation, like vibrations from the surroundings and the shaker itself.

As mentioned the damping of the system was one of the harder parameters to replicate. Given more time, the system would have been designed to better match a real environment, and would likely have a simulation that more accurately imitates the test rig. For instance, the damping

of the system could have been approximated by exposing the cantilever to a pulse, and then curve fitting an envelope function to the diminishing amplitude. Unfortunately, this method was not pursued due to the limited amount of time at the point of discovery, and the damping was set to 0.02, from calculations from material properties and air damping.

Examining *figure 24* and *figure 26* one can observe that the simulated sweep show diminishing peaks following resonance. This is probably a consequence of the dampening as well as the fact that it is a transient measurement. As opposed to the measurements shown in *figure 26*, which are at a steady state.

5.4. Test rig

It is important to consider that this study is addressing a real-life system which includes a living being. Because of the lacking degrees of freedom, the test rig cannot fully provide accurate results, and one must decide on an acceptable amount of uncertainties.

Limitations of the setup

The movement of the vibration shaker is one-dimensional. The movement of the fish on the other hand, is not. Also the temperature and pressure conditions for the test rig, are that of ordinary land based room, whilst the fish dives deeper and have a fluctuating body temperature. There is also the aspect of orientation, since the fish swims freely in the water, the cantilever will not always be in the preferred angle. This was hard to replicate in a lab setup with a horizontal shaker, without specialized equipment. As seen in the paper from Føre [17] the fish rolls and tilts, and its body is usually not on a transverse plane. There is the question of what the effect the tilt or roll would have on the propagated force of the cantilever.

To obtain a more precise damping estimation, one should perform experiments that better mimic fish movement, like a robotic fish or something with a similar range of motions, For example the fish tail used by Cha et al. [7]. The damping of our test rig is measured using an oscilloscope to track the attenuation after giving the cantilever an impulse signal (see *appendix M* for oscilloscope output). The measured damping in the performed tests only accounts for air and material friction, and is therefore presumed lower than that of cantilever inside a real fish.

The shaker was limited to 0.05 Gs for frequencies around 2 to 3 Hz. The electrical energy produced at this excitation and frequency was too little for the multimeter to distinguish it from the surrounding electrical noise. Clear and stable readings were not attained until the frequency reached 4Hz.

Interpreting the measurements

As seen in *table 11*, the lowest resonance frequency that was possible to reach with a reasonable weight was 19 Hz. These results were achieved with Cantilever B and a proof mass of 10 g. Were one to ignore the limit for the weight completely, it could be possible to reach a resonance of 8.15 Hz with the weight of 37.23 g, which at 0.1 Gs (peak) generated 11 VRMS and 21 μ ARMS, open circuit. Undoubtedly, were one to operate either cantilever A or B with a proof mass of this weight, the cantilever itself would probably break.

The measurements for Cantilever B at 19 Hz yielded the results shown in *section 4.3*, *figure 27* and *figure 28*. These findings indicates that there is potential for harvesting mechanical energy that could fulfill the requirements given in *table 7*. The strain caused by the acceleration of 0.1 G seems to be sufficient. However, the frequency is still not within the required range.

Uncertainties

During the testing period it was discovered a number of uncertainties which could have had undesired effects on the measurements. Obvious uncertainties are the estimated stiffness of Cantilever B, which was a known risk. However, thinning down Cantilever B was essential for the experiments, and thus a risk worth taking.

There are also uncertainties connected with random vibrations from the surrounding area of the test rig. Optimally, the shaker would have been fastened to a heavy and rigid surface, like a heavy metal or concrete slab, but acquiring such a station was not feasible at this time.

There were some changes in the resonance between the series, assumably caused by minor differences in the setup between the measurements. Indeed, small adjustments in the clamping position and attachment of the proof mass, change in the center of gravity; all are potential contributions to the changes.

Other possible deviations may be caused by small inaccuracies in the potentiometer. Since the only available way of doing a sweep over the different loads was to use a turning potentiometer, the results were expected to have a few points of error. The potentiometer used seemed to be prone to changing the values due to shaking and vibrations. To counter this, the resistance of the potentiometer was verified between measurements.

Since the cantilever was fastened to the top of the shaker both terminals leading from the EH were suspended in the air during measuring. This was also the case with the accelerometer's leads, which were also mounted on top of the EH. Both sets of cables were secured by being taped to the shaker itself, with some leeway to prevent the leads from damping the oscillations of the base. It is hard to say how much of an impact this would have had on the damping of the system.

Another, not so frequently occurring problem was when the adhesive of the proof mass would start to lose its hold. This only occurred when mounting the heaviest loads onto the tip of the cantilever, which sounds reasonable since more weight equals a larger force. Although the small loss of contact between the cantilever and proof mass was almost too small to register by touch, it is hard to say whether or not this may have caused any nonlinearities that were observed in some of our measurements, but there is a possibility that it had an effect.

5.5. Experiments

Unfortunately the performed set of test are not reproducible, as the flux of the magnets are unknown, in addition to other uncertainties, including mass and acceleration.

The performed experiments can therefore not be validated. Still they indicate that the use of an endstop and/or magnets might have a positive effect. The first round of experiments proved to have serious flaws, as the magnet got stuck to the endstop. The second round was therefore conducted with the same parameters, except for exchanging the magnets for a set of weaker ones. Given more time it would be interesting to investigate this further, to see what can be achieved under more systematic tests, when combining magnets and endstops. More on this in *section 5.7*.

5.6. Other challenges

Administrative challenges

Besides the time limitation, there have been several other administrative challenges following this work, especially when it comes to available workspace and equipment. Unfortunately it was not possible to work from TBs offices, due to COVID restrictions.

Therefore all work in the early stages was done either from home or from different group rooms. As available workspaces at NTNU are limited during normal conditions, the pandemic made the need for space far greater than the available rooms. The student based booking limit, for group rooms and the lack of available workspace, made the day-to-day routine unpredictable and more difficult to manage. Thus, some of the work had to be done from open on-campus areas

The need for a lockable room grew when entering the test period. The needed equipment was quite expensive, and this was therefore set as a criteria upon borrowing. Getting access to a lab area or a lockable workspace proved to be challenging, and in combination with the widespread range of faculties and resources to borrow from, the overall process proved to be time consuming.

Complex interdisciplinary field

Apart from the complex field of marine biology, there are several other disciplines involved. These include material technology and chemistry, mechanical engineering, renewable energy and also electrical engineering. It has therefore been challenging to achieve adequate knowledge on all aspects of design and implementation.

There is also a lack of precise research on harvesting energy from sources with extremely low frequency combined with low acceleration. Especially when taking animal welfare into account. This makes the literature somewhat difficult to navigate and collect. The the amount of literature on piezoelectricity and energy harvesting, on the other hand, can feel overwhelming. Most of the curriculum differs from that of electrical engineering, and combined with few available specific studies, the research became demanding to comprehend.

Ethical aspects

The need for in vivo experiments, and the area of use for the EH, come with some conflicting ethical aspects. On one side implantation of a foreign object could potentially be damaging for the individual animal. On the other side it is important to have knowledge and oversight over the population, especially when it comes to endangered species, which is the case for both AS, and other marine species. It is also important to ensure a high level of sustainability and to reduce the need for environmentally hazardous batteries.

Another aspect that should be addressed is the use of PZT. This material contains lead, which is known to be toxic. Since the beam has a protective coating and also is placed inside a container there's no exposure for the fish, thus the use of PZT is deemed safe until further notice. Still, the environmental impact of possible lead waste in the ocean should be considered.

Regarding the whole process of design and placement, the possible power output comes at the expense of animal welfare and environmental concerns. The main ethical goal must therefore be to achieve an affordable and sustainable balance.

This balance needs to be addressed by scientists with a broader knowledge base, as the biological and behavioral aspects of marine life are difficult to fathom without an in-depth understanding of the field.

The study on biomechanical PEHs can also be usable for other fields, like tracking of other small animals as birds, insects, rodents, etc. There is also broad possibilities in the field of medicine, where the harvester possibly can power lifesaving equipment. One of the studies with a solid research base is that of pacemakers powered by the human heart [8]. There will also be lesser need for batteries, which is both more environmentally friendly and more energy efficient.

As previously mentioned, the data sets for endangered animals will span over a larger period of time, which results in a broader knowledge base for scientists and researchers.

As mentioned, WSNs from TB are implanted, which means that the fish needs to be captured before the node gets surgically implanted. Afterwards the fish needs to be kept

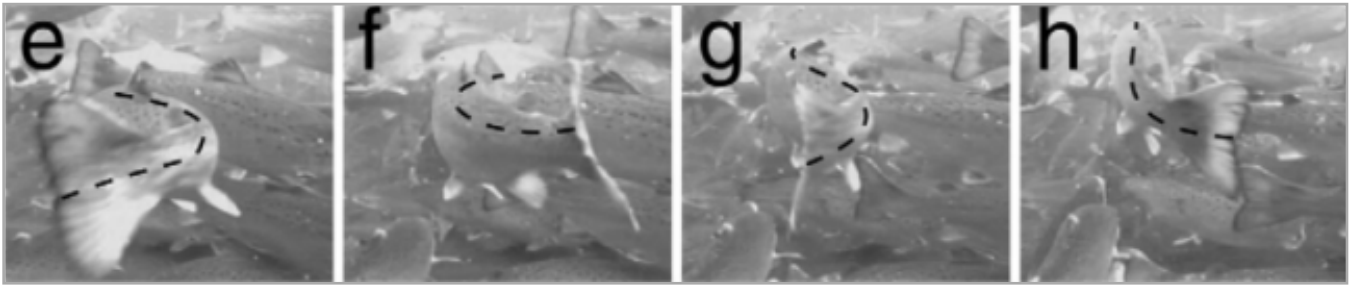


FIGURE 30: Bending of fish tail [17].

in a safe environment to allow healing before it is released back to the wild.

For these devices to be approved, they also need to stay within certain biological boundaries. In Norway these boundaries are determined by Mattilsynet. According to TB and Lennox Mattilsynet mostly focuses on restriction in length, and it was pointed out that the 2% weight rule should be considered more important, since this also affects the fish's buoyancy. These restrictions limit size and weight, but for an PEH, the placement limitations are equally important. Placement of the harvester will determine the propagation of ambient vibration, and therefore also the power outtake.

Another limitation is the unpredictability of the surroundings and behavior of the fish. It is important to remember that the operating environment of the system is placed inside a living being. It's therefore only possible to give predictions from the test rig, as the outtake will vary between sizes, lifestages and species. In vivo experiments are therefore necessary.

5.7. Further work

As repeatedly mentioned, the main challenge with the chosen configuration is to get the resonance of the cantilever to match the low tail beat frequency spectrum from the fish, and to get enough output over an adequate BW to be able to store.

Because of the combination of low frequencies and low acceleration (in average approximately around 0.1 G), the power output is too low. Therefore, it is important to look further, and to investigate other possible configurations for frequency tuning.

One possible solution to the tuning challenge could be reshaping and/or reconfiguring the piezoelectric material. Another possibility is to design a hybrid EH that implements other technologies to enhance the force on the piezoelectric material.

As the results show, there is potential for energy harvesting using piezoelectric materials.

Optimization of simulation model

If the continuation of the cantilever approach is to be pursued there is some additional work that would be beneficial to the current model. A more optimized simulation of the cantilever inside the container could be a big advantage. Our suggestion on how to continue advancing the simulation model would be to incorporate circuit elements that could represent the walls of the container in *figure 14*, similar to how [24] has done with the end-stops. Another valuable addition would be a more detailed representation of the air-damping present when the cantilever oscillates inside the container. Seeing as the current simulation would struggle to incorporate parameters, like pressure and temperature, it is suggested that a multi physics simulator, like COMSOL be tried.

Other materials and configurations

Further work should be put into exploring the possibilities of utilizing the direct bending motion of the fish's tail, as opposed to the vibrations caused by it. Seen in *figure 30* it is a great deal of bending and displacement in that area of the body. To further investigate this approach, the use of robotic fish tail, shown in [7], that could replicate the actual movement of the fish would be of interest. Further work should be conducted into how the attachment of a PEH to live animals affects their movement and comfort. For these kinds of experiments, it is suggested that instead of a stiff

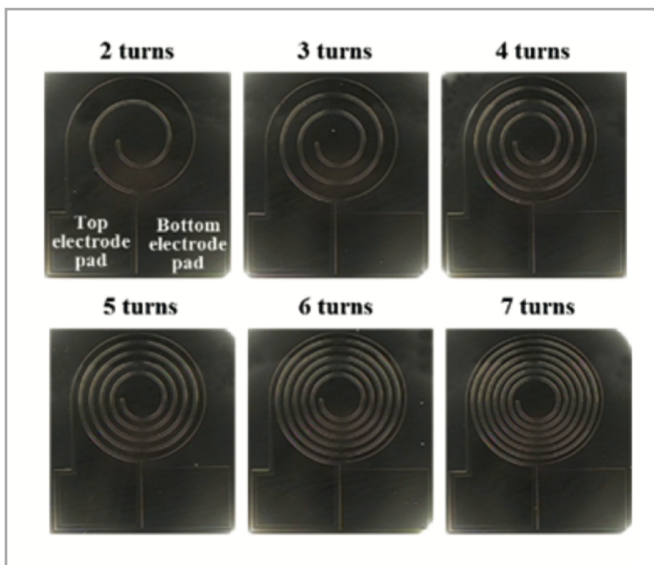


FIGURE 31: Spiral shaped springs with different number of turns [9]

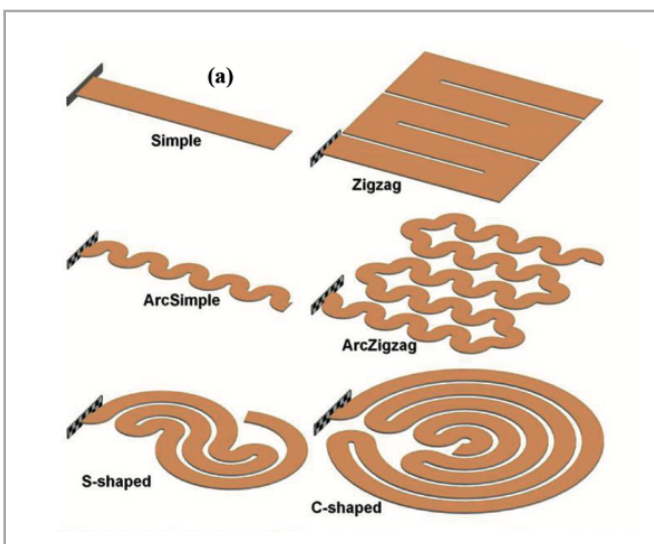
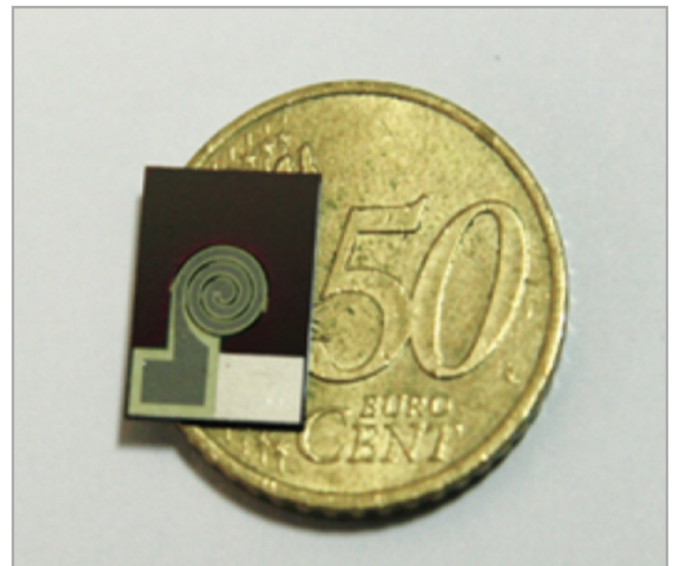


FIGURE 32: Other possible spring shapes [9]

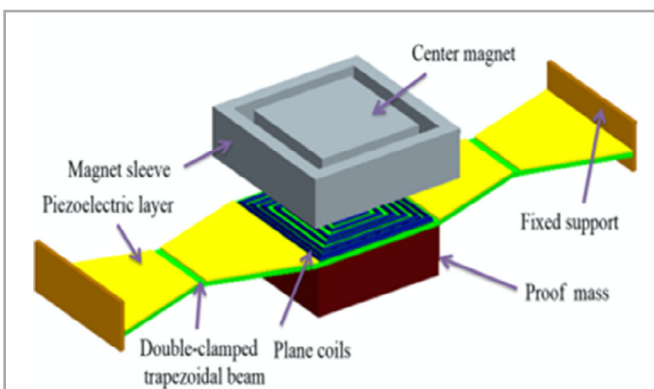


FIGURE 33: Trapezoid piezoelectric beam in a hybrid energy harvester [8]

cantilever a softer material like piezoelectric patches (MFC) available through Smart Materials [25].

As mentioned, stiffness reduction can be done in several ways, for example by choosing a narrower beam size or by reducing the thickness and stiffness of the protection layer. The latter could be more efficient by having a thinner layer in a more elastic material than FR4, in example epoxy/aramid.

Another possibility is to choose another spring shape than the rectangular beam. Alternatives like spirals and other spring shapes like zig zag, arch, C shapes, have proved to have a lower resonance operation [9].

Hybrid energy harvesters

One possibility is to include magnets on both sides of the cantilever's tip. This will provide extra force on the tip mass, and the idea is that the vibrations are affected by the magnetic field. The performed tests have shown that there are tendencies in combination with an endstop, but one must be conscious of the weight limitations. Thus, the power and bandwidth must be high enough to justify the weight of the magnets used. This should be looked further into with a broader timeframe, and more stable and reproducible test environments.

Another hybrid model includes ferroballs, and there are findings that support that this is a possible solution [8]. One must also be conscious of magnets as they can have unwanted effects on electronic circuits. It is therefore important to investigate

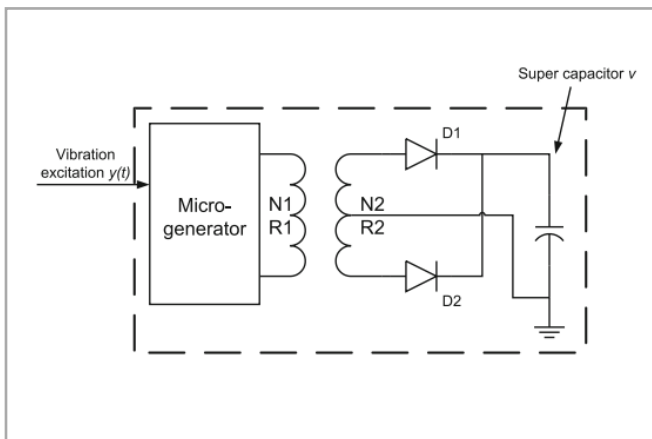


FIGURE 34: Rectifier and voltage transformer

how TB's transmitters would react to being in close proximity to magnets. There is also some research that indicates that the use of ferrofluids can be of interest [9].

Charging circuit

Because the piezoelectric generator has an AC output it must be converted to DC before it can be used to charge a battery or power a circuit. Keep in mind that, for energy harvesters, we want as much power to transfer as possible. Picking the wrong rectifier could work as a bottleneck. For this reason a full wave rectifier is the logical choice over the half wave, which cuts out half the incoming power. Piezos are known for producing high voltage levels. Because of this we need a way to protect other circuit elements from being overloaded and broken. To counter this the circuit should have a voltage regulator (DC/DC) to reduce the levels down to an easier to manage level. There are many designs to choose from when it comes to rectifiers. When choosing a full wave rectifier a model that consists of 2 diodes instead of 4 diodes may be beneficial due to less energy loss. See figure 34.

Use of non-linearities

As shown in the results, the use of endstops can broaden the BW, and also give higher magnitude on the acceleration bursts. Reserach supports the use of endstops. As stated in "A Review on Mechanisms for Piezoelectric-Based Energy Harvesters" [8], the use of non-linearities could contribute in a positive way, both brodening the BW and increasing the output. This is also stated by Blystad and Halvorsen [24], and Priya et. al [9].

Nano electro-mechanical systems

The need for more lightweight sensors is considered to be of greater importance for smaller fish, with weight below 100 grams. Especially in the range 17-30 grams, as stated by Lennox. For fish in this size class, the requirements are harder to meet. Also finding solutions that fit individual cases is not manageable, so possibilities in nanomechanical systems could be of interest.

Assessments of expense

"Piezoelectric MEMS technology is the most cost-effective energy harvesting technology if it can provide high enough power density and wide enough bandwidth" [9].

For an EH to be cleared for production, it is utmost important that it has a low weight, that it is sustainable and that the production cost therefore are justified. See figure 35.

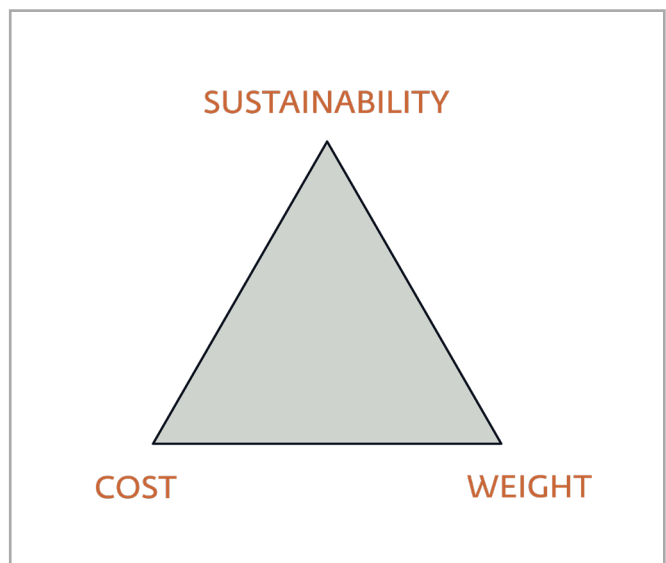


FIGURE 35: Triangle of expense

5.8. Conclusion

This study aimed to investigate the possibilities of using kinetic energy from fish. This technology would be helpful for monitoring the animals over longer periods of time, in turn helping our understanding of their behavior grow. The topic of PEH is vast and the numerous configurations and applications makes it a field with many niches.

The preparational work therefore contained a thorough literature review. The pursued configuration in this study is of a piezoelectric cantilever. This model was chosen because

it's more considerate to the health of the fish, compared to the other methods. Also, replicating the cantilever model is simpler in a lab environment.

The model was tested through simulations, and a physical setup. The physical measurements explore different methods of adjusting the system, like tuning resonance and obtaining optimal load for maximum power transfer. Although, the lack of well suited, commercially available PEH, made it challenging to obtain enough energy output.

The latter part of this study evaluates the results obtained from the measurements and simulation. Here, enhancements to the tested model is suggested and uncertainties are addressed. In addition, other models are presented as interesting alternatives to the piezoelectric cantilever.

Throughout this study, it has become evident that the field of energy harvesting is both complex and important. The goal all along, was to investigate the possible power outtake within the boundaries of animal welfare. The results showed that with the specifications at hand, the output was not at a sufficient level, but still the tendencies showed that the topic needs more research. It is therefore not possible to conclude at this stage, as there seems to be uninvestigated possibilities.

The main hope forward, is that this paper can be an inspiration for others, and that there will be future research on other methods of tuning. Either to achieve more power output from cantilever configuration or to find more animal friendly ways to make use of bending instead of vibrations. Until then ...

"So long, and thanks for all the fish"

REFERENCES

- [1] Thelma Biotel AS (n.d.), Services, Thelma Biotel AS, viewed on 5 february 2021, < <https://www.thelmabiotel.com/service/> >
- [2] Search: <https://www.iucnredlist.org>, see appendix D
- [3] Freyhof, J. 2014. *Salmo salar*. The IUCN Red List of Threatened Species 2014: e.T19855A2532398. Downloaded on 30 May 2021.
- [4] Vøllestad, A. 2021. Laksefamilien. Store norske leksikon on snl.no. Vied 30. mai 2021. <https://snl.no/laksefamilien>
- [5] Iqbal, Muhammad et al., 2021. Vibration-based piezo-electric, electromagnetic, and hybrid energy harvesters for microsystems applications: A contributed review. *International journal of energy research*, 45(1), pp.65–102.
- [6] Li, Huidong et al., 2016. An Energy Harvesting Underwater Acoustic Transmitter for Aquatic Animals. *Scientific reports*, 6(1), p.33804.
- [7] Cha, Youngsu et al., 2016. Energy harvesting from a piezoelectric biomimetic fish tail. *Renewable energy*, 86, pp.449–458.
- [8] Elahi, Hassan, Eugeni, Marco & Gaudenzi, Paolo, 2018. A Review on Mechanisms for Piezoelectric-Based Energy Harvesters. *Energies (Basel)*, 11(7), p.1850.
- [9] Priya, Shashank et al., 2017. A Review on Piezoelectric Energy Harvesting: Materials, Methods, and Circuits. *Energy harvesting and systems*, 4(1), pp.3–39.
- [10] Kim, Sehwan & Chou, Pai H, 2015. Energy harvesting: Energy harvesting with supercapacitor-based energy storage. In *Smart Sensors and Systems*. pp. 215–241.
- [11] Qin, Qinghua, 2013. *Advanced Mechanics of Piezoelectricity* 1. Aufl., Berlin, Heidelberg: Springer-Verlag.
- [12] Carter, Rob & Kensley, Richard (n.d.), Introduction to Piezoelectric Transducers, Piezo.com, viewed 2 march 2021, <<https://piezo.com/pages/intro-to-piezoelectricity>>
- [13] Hehn, Thorsten & Manoli, Yiannos, 2014. Piezoelectricity and Energy Harvester Modelling. In *CMOS Circuits for Piezoelectric Energy Harvesters*. Springer Series in Advanced Microelectronics. Dordrecht: Springer Netherlands, pp. 21–40.
- [14] Anon, *Handbook of Sensors and Actuators*.
- [15] Hehn, Thorsten & Manoli, Yiannos, 2014. Performance Analysis of the PSCE Chip. In *CMOS Circuits for Piezoelectric Energy Harvesters*. Springer Series in Advanced Microelectronics. Dordrecht: Springer Netherlands, pp. 129–185.
- [16] Zhu, Dibin, Tudor, Michael J & Beeby, Stephen P, 2010. Strategies for increasing the operating frequency range of vibration energy harvesters: a review. *Measurement science & technology*, 21(2), p.022001.
- [17] Føre, Martin, Alfredsen, Jo Arve & Gronningsater, Aage, 2011. Development of two telemetry-based systems for monitoring the feeding behaviour of Atlantic salmon (*Salmo salar* L.) in aquaculture sea-cages. *Computers and electronics in agriculture*, 76(2), pp.240–251.
- [18] Senturia, Stephen D, 2007. *Microsystem Design*, Boston, MA: Springer.
- [19] Datasheet: <https://www.bksv.com/-/media/literature/Product-Data/bp0232.ashx>.
- [20] Datasheet, MPU 6050: <http://www.farnell.com/datasheets/1788002.pdf>
- [21] Datasheet, ATmega 328p: https://ww1.microchip.com/downloads/en/DeviceDoc/Atmel-7810-Automotive-Microcontrollers-ATmega328P_Datasheet.pdf
- [22] Transducer: <https://piezo.com/collections/piezoelectric-actuators-motors/products/piezoelectric-bending-transducer-s129-h5fr-1803yb>
- [23] Wikipedia contributors. (2021, May 27). Osmium. In Wikipedia, The Free Encyclopedia. Retrieved 20:39, May 31, 2021, from <https://en.wikipedia.org/w/index.php?title=Osmium&oldid=1025422560>
- [24] Blystad, Lars-Cyril Julin et al., 2011. A piezoelectric energy harvester with a mechanical end stop on one side. *Microsystem Technologies*, 17(4), pp.505–511.
- [25] Mishra, Suvrajyoti et al., 2019. Advances in Piezoelectric Polymer Composites for Energy Harvesting Applications: A Systematic Review. *Macromolecular materials and engineering*, 304(1), pp.1800463-n/a.
- [26] Chen, Yi-Chen, Cheng, Chih-Kun & Shen, Sheng-Chih, 2019. Design and Fabrication of a Displacement Sensor Using Screen Printing Technology and Piezoelectric Nanofibers in d33 Mode. *Sensors and materials*, 31(2), p.233.
- [27] Senturia, S.D., 2001. *Microsystem design*, Boston: Kluwer Academic.
- [28] Adams, Douglas. (2004). *The hitchhiker's guide to the galaxy*. New York, Harmony Books.

APPENDIX

Appendix A: Instruments and components

Instrument/component	Model/Developer	Datasheet
Shaker	BKSV	https://www.bksv.com/-/media/literature/Product-Data/bpo232.ashx
Amplifier	Unknown	
Accelerometer	Sparkfun MPU 6050	https://invensense.tdk.com/wp-content/uploads/2015/02/MPU-6000-Datasheet1.pdf
Multimeter	Fluke	https://dam-assets.fluke.com/s3fs-public/6011663a-no-17x-ds-w.pdf?gVu-a6U7mRtHrVMTKzMsCfJj3k4QjuG
Oscilloscope	Rohde & Schwarz	https://scdn.rohde-schwarz.com/ur/pws/dl_downloads/dl_common_library/dl_brochures_and_datasheets/pdf_1/RTB2000_dat-sw_en_3607-4270-22_v1500.pdf
Multimeter	Rohde & Schwarz	https://scdn.rohde-schwarz.com/ur/pws/dl_downloads/dl_common_library/dl_brochures_and_datasheets/pdf_1/HAMEG_DB_EN_HMC8012.pdf
Function generator	Rohde & Schwarz	https://scdn.rohde-schwarz.com/ur/pws/dl_downloads/dl_common_library/dl_brochures_and_datasheets/pdf_1/HMF25xx_EN_Vo2_Datasheetpdf.pdf
Arduino UNO (ATmega 328p)	Arduino/Atmel	https://ww1.microchip.com/downloads/en/DeviceDoc/Atmel-7810-Automotive-Microcontrollers-ATmega328P_Datasheet.pdf
S129-H5FR-1803YB	Midé	https://www.mouser.com/datasheet/2/606/ppa-piezo-product-datasheet-844547.pdf
Potentiometer	-	-































Appendix B: Software

Program	Comment
LTspice	Simulation of equivalent circuit
MATLAB	All plots and analysis
Arduino IDE	Accelerometer code
ComPort	Reading and exporting from data set B
PuTTY	Output program for Accelerometer
Excel	Used to create csv files for dataset A
Comsol	Multiphysics simulation of cantilever, too complex and timeconsuming to be included in this paper

Appendix C: Online resources

Name	URL
Thelma Biotel	https://www.thelmabiotel.com
Piezo.com	https://piezo.com/
LearnPiezo	https://www.learnpiezo.com
Oria	http://ntnu.oria.no
Wikipedia	https://www.wikipedia.org
Store Norsk Leksikon	https://snl.no
ResearchGate	https://www.researchgate.net
Science Direct	https://www.sciencedirect.com
Google Scholar	https://scholar.google.com/
IUCN Redlist	https://www.iucnredlist.org/search/grid?query=salmon&searchType=species
Library: MPU-6050	https://github.com/jarzebski/Arduino-MPU6050
Library: statistics	https://github.com/RobTillaart/Statistic

Appendix D: Screenshot from IUCN

<p>ANIMALIA - ACTINOPTERYGII GLOBAL</p> <p>Sockeye Salmon <i>Oncorhynchus nerka</i> COOK INLET</p> <p>— Stable </p>	<p>ANIMALIA - ACTINOPTERYGII GLOBAL</p> <p>Sockeye Salmon <i>Oncorhynchus nerka</i> NASS-SKEENA ESTUARY: North of Nass</p> <p>↓ Decreasing </p>	<p>ANIMALIA - ACTINOPTERYGII GLOBAL</p> <p>Sockeye Salmon <i>Oncorhynchus nerka</i> COLUMBIA RIVER: Upper, Headwater/Arrow, Whatsan Lk</p> <p></p>
<p>ANIMALIA - ACTINOPTERYGII GLOBAL</p> <p>Sockeye Salmon <i>Oncorhynchus nerka</i> WESTERN KAMCHATKA CURRENT (WARM)</p> <p>— Stable </p>	<p>ANIMALIA - ACTINOPTERYGII GLOBAL</p> <p>Sockeye Salmon <i>Oncorhynchus nerka</i> SKEENA R, MIDDLE: Nanika Lk/Morice R</p> <p>↓ Decreasing </p>	<p>PLANTAE - MAGNOLIOPSIDA GLOBAL</p> <p>Salmon Bean <i>Archidendron vaillantii</i></p> <p>Unknown </p>
<p>ANIMALIA - ACTINOPTERYGII GLOBAL</p> <p>Sockeye Salmon <i>Oncorhynchus nerka</i> PRINCE WILLIAM SOUND</p> <p>↑ Increasing </p>	<p>ANIMALIA - ACTINOPTERYGII EUROPE</p> <p>Blackhead Salmon <i>Narcetes stomias</i></p> <p>— Stable </p>	<p>ANIMALIA - ACTINOPTERYGII GLOBAL</p> <p>Blackhead Salmon <i>Narcetes stomias</i></p> <p>— Stable </p>
<p>ANIMALIA - CHONDRICHTHYES GLOBAL</p> <p>Salmon Shark <i>Lamna ditropis</i></p> <p>— Stable </p>	<p>ANIMALIA - ACTINOPTERYGII GLOBAL</p> <p>Sockeye Salmon <i>Oncorhynchus nerka</i> ANADYR CURRENT</p> <p>Unknown </p>	<p>ANIMALIA - ACTINOPTERYGII GLOBAL</p> <p>Sockeye Salmon <i>Oncorhynchus nerka</i> FRASER RIVER, MIDDLE: Nadina, Nechako (early summer)</p> <p>↑ Increasing </p>
<p>ANIMALIA - ACTINOPTERYGII GLOBAL</p> <p>Sockeye Salmon <i>Oncorhynchus nerka</i> COLUMBIA RIVER: Redfish Lk</p> <p>↓ Decreasing </p>	<p>ANIMALIA - ACTINOPTERYGII GLOBAL</p> <p>Sockeye Salmon <i>Oncorhynchus nerka</i> PUGET SOUND-GEORGIA BASIN: Schoen Ck/Davie R</p> <p>Unknown </p>	<p>ANIMALIA - ACTINOPTERYGII GLOBAL</p> <p>Sockeye Salmon <i>Oncorhynchus nerka</i> NASS-SKEENA ESTUARY: Hugh Smith Lk/Boca de Quadra</p> <p>↓ Decreasing </p>
<p>ANIMALIA - ACTINOPTERYGII GLOBAL</p> <p>Sockeye Salmon <i>Oncorhynchus nerka</i> HECATE STRAIT-Q.C. SOUND: Lowe Lk/Granville Ch</p> <p>↓ Decreasing </p>	<p>ANIMALIA - ACTINOPTERYGII GLOBAL</p> <p>Sockeye Salmon <i>Oncorhynchus nerka</i> VELIKAYA RIVER</p> <p>Unknown </p>	<p>ANIMALIA - ACTINOPTERYGII GLOBAL</p> <p>Sockeye Salmon <i>Oncorhynchus nerka</i> COPPER RIVER</p> <p>↑ Increasing </p>
<p>ANIMALIA - ACTINOPTERYGII GLOBAL</p> <p>Sockeye Salmon <i>Oncorhynchus nerka</i> SKEENA R, LOWER: McDonnell Lk/Zymoetz R</p> <p>Unknown </p>	<p>ANIMALIA - ACTINOPTERYGII GLOBAL</p> <p>Sockeye Salmon <i>Oncorhynchus nerka</i> TRANSBOUNDARY FJORDS: Kah Sheets Lk/S Kupreanof Is</p> <p>Unknown </p>	<p>ANIMALIA - ACTINOPTERYGII GLOBAL</p> <p>Sockeye Salmon <i>Oncorhynchus nerka</i> FRASER RIVER, LOWER: Upper Pitt R (early summer)</p> <p>↑ Increasing </p>
<p>ANIMALIA - ACTINOPTERYGII GLOBAL</p> <p>Sockeye Salmon <i>Oncorhynchus nerka</i> HECATE STRAIT-Q.C. SOUND: Kitimat to Kitlope R</p> <p>— Stable </p>	<p>ANIMALIA - ACTINOPTERYGII GLOBAL</p> <p>Sockeye Salmon <i>Oncorhynchus nerka</i> HECATE STRAIT-Q.C. SOUND: Queen Charlotte Sound</p> <p>↓ Decreasing </p>	<p>ANIMALIA - ACTINOPTERYGII GLOBAL EUROPE</p> <p>Danube salmon <i>Hucho hucho</i></p> <p>Unknown </p>
<p>ANIMALIA - ACTINOPTERYGII GLOBAL</p> <p>Sockeye Salmon <i>Oncorhynchus nerka</i> TRANSBOUNDARY FJORDS: North</p> <p>— Stable </p>	<p>ANIMALIA - ACTINOPTERYGII GLOBAL</p> <p>Sockeye Salmon <i>Oncorhynchus nerka</i> COLUMBIA RIVER: Okanogan R/Osoyoos Lk</p> <p>↑ Increasing </p>	<p>ANIMALIA - ACTINOPTERYGII GLOBAL</p> <p>Sockeye Salmon <i>Oncorhynchus nerka</i></p> <p>— Stable </p>
<p>ANIMALIA - ACTINOPTERYGII GLOBAL</p> <p>Sockeye Salmon <i>Oncorhynchus nerka</i> PUGET SOUND-GEORGIA BASIN: Baker Lk/Puget Sound</p> <p>↑ Increasing </p>	<p>ANIMALIA - ACTINOPTERYGII GLOBAL</p> <p>Sockeye Salmon <i>Oncorhynchus nerka</i> SKEENA R, UPPER</p> <p>↓ Decreasing </p>	<p>ANIMALIA - ACTINOPTERYGII GLOBAL</p> <p>Sockeye Salmon <i>Oncorhynchus nerka</i> COLUMBIA RIVER: Wallowa Lk</p> <p></p>

<https://www.iucnredlist.org/search/grid?query=salmon&searchType=species>

Appendix E: Physical properties for TB's transmitters

Physical properties for 6, 7, 9, 13 and 16 transmitter series												
	LP6	2LP6	LP7	2LP7	MP7	LP9L	MP9	MP9L	LP13	2LP13	MP13	HP16
Diameter	6.3	6.3	7.3	7.3	7.3	9	9	9	12.7	12.7	12.7	16
Length	14.5	22	17	23.2	20.6	24	24.4	29.4	27.9	38.7	33.3	70
Weight (air)	1.2	1.9	1.8	2.7	2.3	4	3.6	5.2	9.19	13.8	11.5	29
Weight	0.7	1.2	1.1	1.8	1.5	2.5	2.1	3.3	5.5	8.7	7.1	14.9

Appendix F: Battery lifespan of TB's transmitters

Battery lifespan for 6, 7, 9, 13 and 16 transmitter series												
Interval	LP6	2LP6	LP7	2LP7	MP7	LP9L	MP9	MP9L	LP13	2LP13	MP13	HP16
30	70 days	139 days	101 days	6 months	69 days	11 months	137 days	7 months	19 months	38 months	14 months	32 months
60	118 days	7.7 months	152 days	11 months	122 days	18 months	7 months	13 months	33 months	66 months	25 months	62 months
90	5 months	10 months	7 months	14 months	5 months	23 months	10 months	17 months	43 months	87 months	35 months	89 months
120	5.9 months	11.8 months	8 months	16 months	6 months	27 months	12 months	21 months	52 months	105 months	43 months	114 months

Appendix G: Activity and tilt calculations (1)

ACOUSTIC TRANSMITTER

ACTIVITY AND TILT

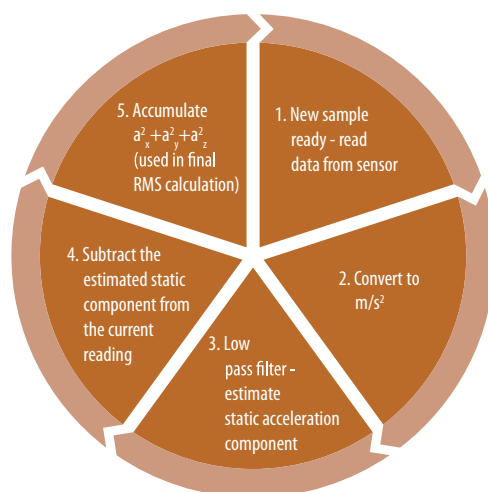
The embedded ultralow power 3-axis accelerometer registers both static and dynamic acceleration with 0.01 m/s² resolution. Common applications are measuring tilt angle of objects or animals, or level of activity. It may even be programmed to detect and report specific motion patterns.

ACTIVITY LEVEL

One central feature of the activity transmitter is its ability to register the level of activity to which it is exposed, like what is found in modern pace counters and activity trackers. This is accomplished by rapid sampling and monitoring the changes in acceleration on the transmitter over time.

On-board Processing Algorithm

Raw acceleration data is sampled from the accelerometer at the desired frequency, converted to m/s², and then passed through a low-pass filter to determine static components such as gravity or other offsets. This provides a static acceleration vector to which the current data sample is compared to extract the acceleration dynamics.



SPECIFICATIONS

Activity

Range activity:	0-3.465 m/s ²
Resolution:	0.01 m/s ²
Sampling frequency:	5 Hz
Max survival depth:	500 m

Tilt

Range tilt:	0-180°
Resolution:	1°
Max survival depth:	500 m

Sensor Combinations



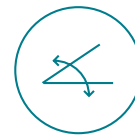
DEPTH



TEMPERATURE



ACTIVITY



TILT

THELMABIOTEL
www.thelmabiotel.com

Activity and tilt calculations (2)

Rotational movement causes changes in the static acceleration vector, and will as such be detected as activity along with linear accelerations. For persisting rotational movement, the influence will be less dominant over time as the low pass filter updates the static acceleration vector estimate. It is possible to tune the strength of the filter by adjusting the cut-off frequency. By default, this is set to 0.2 Hz.

The acceleration dynamics are accumulated over the desired sampling duration, and then a Root Mean Square (RMS) value of the acceleration is calculated. A_{RMS} is the value transmitted by the tag, and provides an estimate of total activity/movement during the sampling window.

$$A_{RMS} = \sqrt{\frac{\sum_{n=1}^N a_x^2 + a_y^2 + a_z^2}{N}}$$

As the characteristics of the activity may vary significantly between use cases the value transmitted by the tag can be programmed with user defined parameters:

- **Sample window duration:** The acceleration sample window is started right after the previous transmit has completed. To make sure the sampling has time to finish before the next transmit, the sampling window should be less than $t_{x_{min}}$.
- **Sample frequency:** Number of acceleration samples (each sample consists of 3 data points – a_x , a_y and a_z) collected in one second. Default sampling frequency is 5 Hz.
- **A_{RMS} acceleration range:** S256 transmits contains 1 byte of sensor data [0-255]. For example, a resolution of 0.013588 m/s² gives a range of 0 - 3.465 m/s². The range has proven useful for smaller and larger pelagic fish species as well as different species of crustaceans.

TILT ANGLE / INCLINATION

The sensor can measure tilt angle along the central axis (default) of the casing. This can be convenient for remote monitoring of tilt angle of any animal, equipment or any other object under water. The transmitted value ranges from 0° to 180°, with a 1° resolution and accuracy.

By using a magnet command the angular zero point may be set to change the default orientation or compensate for misalignment after mounting the tag.

BEHAVIOUR SIGNATURE RECOGNITION

Another key feature of the activity transmitter is the capability of detecting various motion signatures based on the raw data from the 3-axis accelerometer. Detection algorithms can be tailored to meet your specific needs and developed by Thelma Biotel. Ideally this is based on real data and video from controlled conditions where the relevant specimen is set up to log data directly from the desired motion pattern. After logging data on the specimen under controlled conditions, typically with video recording, the data can be analysed and used during programming.

Appendix H: Data set examples (1)

Data set A

Date	Time	Tilt	Roll	Ax	Ay	Az
01-10-09	09:23:58.000	132	65	0	-33	-24
01-10-09	09:23:58.050	131	65	-42	14	183
01-10-09	09:23:58.100	131	65	31	-12	7
01-10-09	09:23:58.150	131	65	0	-16	-1
01-10-09	09:23:58.200	131	65	1	-21	-13
01-10-09	09:23:58.250	131	65	0	-18	6
01-10-09	09:23:58.300	131	65	0	-4	12
01-10-09	09:23:58.350	130	65	0	-12	16
01-10-09	09:23:58.400	130	65	1	-3	6
01-10-09	09:23:58.450	130	65	1	-21	1
01-10-09	09:23:58.500	130	65	0	-7	-4
01-10-09	09:23:58.550	130	65	0	-12	7
01-10-09	09:23:58.600	130	65	0	-9	0
01-10-09	09:23:58.650	130	65	0	-6	10
01-10-09	09:23:58.700	130	65	0	-10	4
01-10-09	09:23:58.750	130	65	-1	-1	17
01-10-09	09:23:58.800	130	65	0	-5	5
01-10-09	09:23:58.850	130	65	0	-11	1
01-10-09	09:23:58.900	130	65	0	0	18
01-10-09	09:23:58.950	130	65	0	-4	11
01-10-09	09:23:59.000	130	65	0	-13	0
01-10-09	09:23:59.050	130	65	0	-1	17
01-10-09	09:23:59.100	130	65	0	-9	0
01-10-09	09:23:59.150	130	65	1	-13	-3
01-10-09	09:23:59.200	130	65	0	-14	-8
01-10-09	09:23:59.250	130	65	0	-5	2
01-10-09	09:23:59.300	130	65	0	-12	3
01-10-09	09:23:59.350	130	65	0	-3	3
01-10-09	09:23:59.400	130	65	0	-10	14
01-10-09	09:23:59.450	130	65	0	-13	-3
01-10-09	09:23:59.500	130	65	0	0	2
01-10-09	09:23:59.550	130	65	0	-8	-2
01-10-09	09:23:59.600	130	65	1	-5	5
01-10-09	09:23:59.650	130	65	0	-18	0
01-10-09	09:23:59.700	130	65	0	0	17
01-10-09	09:23:59.750	130	65	1	-1	4

Data set examples (2)

Data set B

Date and Time (UTC)	Unix Timestamp (UTC)	ID	Data	Protocol	SNR	Receiver
2021-01-21T08:18:25.364Z	1611217105.364	3038	17	S64K-71kHz	10	1503
2021-01-20T23:56:25.765Z	1611186985.765	3038	15	S64K-71kHz	23	1503
2021-01-20T23:49:34.756Z	1611186574.756	3038	15	S64K-71kHz	27	1503
2021-01-20T23:45:15.749Z	1611186315.749	3038	17	S64K-71kHz	32	1503
2021-01-20T23:42:57.747Z	1611186177.747	3038	19	S64K-71kHz	28	1503
2021-01-20T23:39:34.745Z	1611185974.745	3038	17	S64K-71kHz	27	1503
2021-01-20T23:37:20.742Z	1611185840.742	3038	15	S64K-71kHz	22	1503
2021-01-20T20:12:02.569Z	1611173522.569	3038	17	S64K-71kHz	19	1503
2021-01-20T20:08:39.566Z	1611173319.566	3038	13	S64K-71kHz	25	1503
2021-01-20T20:02:57.561Z	1611172977.561	3038	17	S64K-71kHz	17	1503
2021-01-20T19:49:16.547Z	1611172156.547	3038	13	S64K-71kHz	19	1503
2021-01-20T19:16:05.508Z	1611170165.508	3038	11	S64K-71kHz	21	1503
2021-01-20T19:10:35.503Z	1611169835.503	3038	11	S64K-71kHz	21	1503
2021-01-20T19:01:05.492Z	1611169265.492	3038	13	S64K-71kHz	20	1503
2021-01-20T18:58:08.490Z	1611169088.490	3038	18	S64K-71kHz	15	1503
2021-01-20T18:48:08.475Z	1611168488.475	3038	13	S64K-71kHz	19	1503
2021-01-20T18:45:04.473Z	1611168304.473	3038	16	S64K-71kHz	17	1503
2021-01-20T17:48:26.417Z	1611164906.417	3038	14	S64K-71kHz	23	1503
2021-01-20T16:08:33.303Z	1611158913.303	3038	15	S64K-71kHz	32	1503
2021-01-20T16:06:14.301Z	1611158774.301	3038	12	S64K-71kHz	32	1503
2021-01-20T16:06:07.817Z	1611158767.817	3038	12	S64K-71kHz	21	1502
2021-01-20T16:04:09.299Z	1611158649.299	3038	14	S64K-71kHz	29	1503
2021-01-20T16:04:02.815Z	1611158642.815	3038	14	S64K-71kHz	23	1502
2021-01-20T16:01:09.296Z	1611158469.296	3038	12	S64K-71kHz	25	1503
2021-01-20T16:01:02.812Z	1611158462.812	3038	12	S64K-71kHz	25	1502
2021-01-20T15:54:09.806Z	1611158049.806	3038	18	S64K-71kHz	13	1502
2021-01-20T15:51:11.286Z	1611157871.286	3038	15	S64K-71kHz	26	1503
2021-01-20T15:51:04.804Z	1611157864.804	3038	15	S64K-71kHz	20	1502
2021-01-20T15:48:14.282Z	1611157694.282	3038	14	S64K-71kHz	27	1503
2021-01-20T15:48:07.802Z	1611157687.802	3038	14	S64K-71kHz	20	1502
2021-01-20T15:44:20.278Z	1611157460.278	3038	11	S64K-71kHz	24	1503
2021-01-20T15:44:13.803Z	1611157453.803	3038	11	S64K-71kHz	15	1502
2021-01-20T15:37:28.266Z	1611157048.266	3038	17	S64K-71kHz	25	1503
2021-01-20T15:34:22.254Z	1611156862.254	3038	10	S64K-71kHz	22	1503
2021-01-20T15:34:15.779Z	1611156855.779	3038	10	S64K-71kHz	13	1502
2021-01-20T15:30:15.249Z	1611156615.249	3038	9	S64K-71kHz	34	1503

Appendix I: Symbols used in piezo compendium (1)



TABLE 5. LIST OF SYMBOLS, CONTINUED

Symbol	Name	Unit
Q_s	Short circuit charge	C
R	Electrical resistance	Ω
s_{ij}^E (i=1 to 6) (j=1 to 6)	Elastic compliance at constant E	m^2 / N
s_{ij}^D (i=1 to 6) (j=1 to 6)	Elastic compliance at constant D	m^2 / N
S_i (i=1 to 6)	Strain components	
S_{max}	Maximum recommended strain	
t	Time	s
t	Response time	s
t	Thickness	m
r		
T_i (i=1 to 6)	Stress components	N / m^2
V	Volume	m^3
V_o	Open circuit voltage	V
v_s	Velocity of sound	m / s
x	Deflection	m
x_o	Free deflection	m
	Thermal expansion coefficient	1 / K
ϵ_0	Dielectric constant of free space	F / m
	Density	kg / m^3
	Electrical bulk resistivity	Ω/m

Symbols used in piezo compendium (2)



TABLE 5. LIST OF SYMBOLS

Symbol	Name	Unit
A	Area	m ²
C	Capacitance	F
D	Diameter	m
D _i	(i=1 to 3) Dielectric displacement	C / m ²
d _{ij}	(i=1 to 3) (j=1 to 6) Piezoelectric charge constants	C / N
E _i	(i=1 to 3) Electric field components	V / m
E _c	Coercive field	V / m
F _r	Resonant frequency	kHz
F	Force	N
F _b	Blocking Force	N
g _{ij}	(i=1 to 3) (j=1 to 6) Piezoelectric voltage constants	V m / N
G	Shear modulus	N / m ²
k	Electromechanical coupling coefficient	
k ₃₃	Longitudinal coupling coefficient	
k ₃₁	Transverse coupling coefficient	
k ₁₅	Shear coupling coefficient	
k _p	Planar coupling coefficient	
k _t	Thickness coupling coefficient	
k _{eff}	Effective coupling coefficient	
K ^S	(i=1 to 3) (j=1 to 3) Relative dielectric constant at constant strain	
K ^T	(i=1 to 3) (j=1 to 3) Relative dielectric constant at constant stress	
L	Length	m
p	Pressure	N / m ²
p	Pyroelectric coefficient	C / m ² K
P _i	(i=1 to 3) Polarization components	C / m ²
P	Power	W
Q	Mechanical quality factor	
Q	Electric charge	C

Appendix J: Material properties for PZT-5# (1)


**TABLE 2. PIEZOELECTRIC AND MATERIAL PROPERTIES FOR PZT-5H, PZT-5A, and PZT-5J
PIEZOCERAMIC**

Property	Symbol	Units	Material Type		
			PZT-5H 3203HD	PZT-5A 3195HD	PZT-5J 3222HD
Dielectric Constant (1kHz)	K^T_3		3200	1900	2650
Dielectric Loss Factor (1kHz)	$\text{Tan}\delta_e$	%	2.0	0.02	0.02
Dielectric Constant (1kHz)	K^T_1			1600	2948
Clamped Dielectric Constant	K^S_3		1200	900	800
Density	ρ	g/cm^3	7.87	7.95	7.90
Curie Point	T_c	$^{\circ}\text{C}$	225	350	270
Mechanical Quality Factor	Q_m		30	80	80
Coercive Field (Measured < 1Hz)	E_c	kV/cm	8.0	12.0	
Remanent Polarization	P_r	$\mu\text{Coul/cm}^2$	39.0	39.0	
Coupling Coefficients	k_p		0.75	0.68	0.72
	k_{33}		0.75	0.72	0.74
	k_{31}		0.43	0.40	0.45
	k_t		0.55	0.49	0.53
	k_{15}		0.78	0.61	0.77
Piezoelectric Charge (Displacement Coefficient)	d_{31}	$\text{Coul/N} \times 10^{-12}$	-320	-190	-270
	d_{33}		650	390	485
	d_{15}	$\text{m/V} \times 10^{-12}$	1000	460	850
Piezoelectric Voltage Coefficient (Voltage Coefficient)	g_{31}		-9.5	-11.3	-11.5
	g_{33}	$\text{V} \cdot \text{m/N} \times 10^{-3}$	19.0	23.2	21.3
	g_{15}		35.3	32.4	32.6
Frequency Constants Radial	N_r	$\text{kHz} \cdot \text{cm}$			191
Resonant Thickness	N_{tr}	$\text{kHz} \cdot \text{cm}$	202	211	205
Anti-Resonant Thickness	N_{ta}	$\text{kHz} \cdot \text{cm}$	236	236	235

Material properties for PZT-5# (2)



TABLE 2. PIEZOELECTRIC AND MATERIAL PROPERTIES FOR PZT-5H, PZT-5A, and PZT-5J PIEZOCERAMIC, CONTINUED

Property	Symbol	Units	Material Type		
			PZT-5H 3203HD	PZT-5A 3195HD	PZT-5J 3222HD
Thermal Expansion (Perpendicular to Poling)	α	ppm/°C	3.5	3.0	
Specific Heat	C_p	J/kg · °C	420	440	
		J/mol · °C	138	145	
Thermal Conductivity with Au Electrodes	K_d	W/cm · °C	1.9-2.3	1.9-2.3	
		W/m · °K	1.2	1.2	
		W/m · °K	1.45	1.45	
Poisson's Ratio	ν		0.31	0.34	0.31
Elastic Constants Short Circuit	S_{11}^E	$\times 10^{-12}m^2/N$	16.6	15.1	15.8
	S_{33}^E		21.0	18.6	18.8
	S_{12}^E			-4.8	-5.0
	S_{13}^E			-7.6	-7.7
	S_{55}^E		52.4	40.0	47.0
Elastic Constants Open Circuit	S_{11}^D	$\times 10^{-12}m^2/N$	13.9	12.7	12.6
	S_{33}^D		8.8	9.0	8.5
	S_{55}^D		20.5	25.1	19.1
Elastic Constants Short Circuit	Y_{11}^E	$\times 10^{10}N/m^2$	6.2	6.6	6.4
	Y_{33}^E		4.9	5.4	5.3
Elastic Constants Open Circuit	Y_{11}^D	$\times 10^{10}N/m^2$	7.0	7.9	7.9
	Y_{33}^D		11.0	11.1	11.7

Appendix K: Piezoelectric configurations



TABLE 3. SPECTRUM OF COMMON PIEZOELECTRIC TRANSDUCERS

PIEZOELECTRIC CONFIGURATION	FREE DEFLECTION	BLOCKED FORCE	RESONANT FREQUENCY	GENERAL FEATURES
	CANTILEVER BENDING MOTOR			5 mm 10 - 500 grams 10 - 500 Hz \$1 - \$100
	$\frac{3 d_{31} L^2 E}{2 T}$	$\frac{3 d_{31} Y b T^2 E}{8 L}$	$\frac{.16 T}{L^2} \sqrt{\frac{Y_{11}}{\rho}}$	
	SIMPLE BENDING MOTOR			↑ INCREASING DISPLACEMENT ↑ INCREASING FORCE ↑ INCREASING RESONANT FREQUENCY ↑ INCREASING COST
	$\frac{3 d_{31} L^2 E}{8 T}$	$\frac{3 d_{31} Y b T^2 E}{2 L}$	$\frac{.48 T}{L^2} \sqrt{\frac{Y_{11}}{\rho}}$	
	TRANSVERSE (D31) CONTRACTION MOTOR			
	$d_{31} L E$	$d_{31} Y A E$ where $A = b T$	$\frac{1}{2 L} \sqrt{\frac{Y_{11}}{\rho}}$	
	LONGITUDINAL (D33) EXTENSION MOTOR			
	$d_{33} L E$	$d_{33} Y A E$ where $A = a b$	$\frac{1}{2 L} \sqrt{\frac{Y_{33}}{\rho}}$	
	SHEAR MODE MOTOR			↓ μm ↓ 10 ³ Kg ↓ 1 MHz ↓ \$100
	$d_{15} T E$	$d_{15} G A E$ where $A = b L$	$\frac{1}{2 T} \sqrt{\frac{Y_{55}}{\rho}}$	

Appendix L: Midé Energy Harvester information (1)



2.0 PRODUCT DATA

2.6 PRODUCT: PPA-1021

The PPA-1021 is a single layer product recommended for energy harvesting and sensing applications. It also exhibits good performance as a resonant actuator. It is not recommended for applications requiring high force output. This is a good cost effective alternative over some of the other products.

DESCRIPTION

Performance data for the PPA-1021 is summarized in the following tables and plots. Refer to Section 6 for information on how this data was gathered. Please note that this data is to be used only as reference and that there is some variability from unit to unit. Temperature, clamp conditions, drive quality, all can contribute to additional variability. All test data was gathered at room temperature and with the PPA-9001 clamp kit hardware.

SPECIFICATIONS

Overview		
Capacitance (nF)		22
Mass (g)		1.4
Full Scale Voltage Range (V)		±200

Layer Material	Thickness (mils)	Thickness (mm)
FR4	3.0	0.08
Copper	1.4	0.03
PZT 5H	10.0	0.25
Copper	1.4	0.03
FR4	14.0	0.36
Total	29.0	0.74

1Information on material properties is provided in Section 5.

2The layer thicknesses do not perfectly add up to the actual thickness of the product due to the epoxy layers. These epoxy layers can be ignored for finite element analysis however.

Stiffness			
Parameter	Clamp -6	Clamp 0	Clamp 6
Effective Stiffness (N/m)	211.60	261.21	442.60
Effective Mass (g)	0.301	0.156	0.233
Max Peak to Peak Deflection (mm)	12.0	11.0	9.0

See Section 4.3 for more information on how to use this data to tune your piezo.

DIMENSIONS

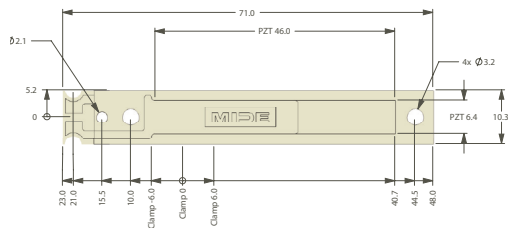


Figure 45: The overall dimensions (mm) for the PPA-1021 are shown. The total thickness is 0.74 mm (29 mils).



Midé Energy Harvester information (2)



2.0 PRODUCT DATA

SPECIFICATIONS

Energy Harvesting Data for Middle Clamp Location									
Acceleration Amplitude (g)	Frequency (Hz)	Tip Mass (gram)	RMS Power (mW)	RMS Voltage (V)	RMS Current (mA)	Resistance (k Ω)	RMS Open Circuit	Peak to Peak Displacement (mm)	Peak to Peak Displacement (in)
0.25	175.0	0.0	0.0	1.2	0.0	47.3	2.1	0.6	0.02
0.50	174.0	0.0	0.1	2.3	0.0	51.9	3.5	0.9	0.04
1.00	173.0	0.0	0.3	3.6	0.1	44.5	5.9	1.5	0.06
2.00	171.0	0.0	0.9	5.6	0.2	35.1	9.8	2.5	0.10
0.25	60.0	1.8	0.2	4.1	0.0	82.5	7.2	1.5	0.06
0.50	60.0	1.7	0.7	8.6	0.1	113.9	14.3	2.9	0.11
1.00	60.0	1.7	1.6	14.0	0.1	125.1	20.5	5.4	0.21
2.00	60.0	1.7	4.4	23.2	0.2	122.9	32.2	8.9	0.34
0.25	23.0	12.7	1.3	17.8	0.1	250.6	27.3	6.5	0.25
0.50	23.0	12.7	2.3	23.3	0.1	232.5	35.5	8.8	0.33
1.00	22.0	12.7	4.5	28.2	0.2	174.9	46.8	16.1	0.59

Block Force and Static Displacement, 100 volt signal			
Parameter	Clamp -6	Clamp 0	Clamp 6
Block Force Amplitude (N)	0.06	0.06	0.09
Displacement Amplitude (mm)	0.24	0.23	0.20

Dynamic displacement, no added tip mass, +/- 100 volt signal			
Parameter	Clamp -6	Clamp 0	Clamp 6
Resonant Frequency (Hz)	133.5	174.3	219.5
Half Power Bandwidth (Hz)	4.0	6.8	19.6
Q Factor	33.4	25.6	11.2
Peak to Peak Deflection at Resonance (mm)	9.8	8.5	4.5
Quasi Static Peak to Peak Deflection (mm)	0.5	0.4	0.3

Dynamic Displacement, 9.3 tip mass, +/- 100 volt signal			
Parameter	Clamp -6	Clamp 0	Clamp 6
Resonant Frequency (Hz)	39.7	48.8	58.0
Half Power Bandwidth (Hz)	1.8	1.6	3.0
Q Factor	22.1	30.5	19.3
Peak to Peak Deflection at Resonance (mm)	11.5	11.0	8.3
Quasi Static Peak to Peak Deflection (mm)	0.5	0.4	0.5

Midé Energy Harvester information (3)



2.0 PRODUCT DATA

Sensitivity, middle clamp, no added tip mass	
Sensitivity (mV/g)	146
Upper Frequency Limit (Hz)	98.0
Resonance (Hz)	182.0
Sensitivity at Resonance (V/g)	7.4

PLOTS

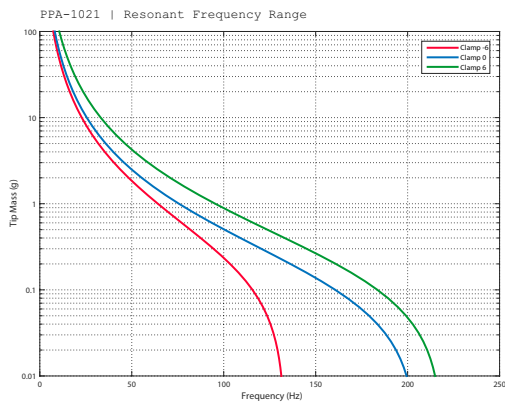


Figure 46: Refer to Section 4.3 for more information on tuning your piezo.

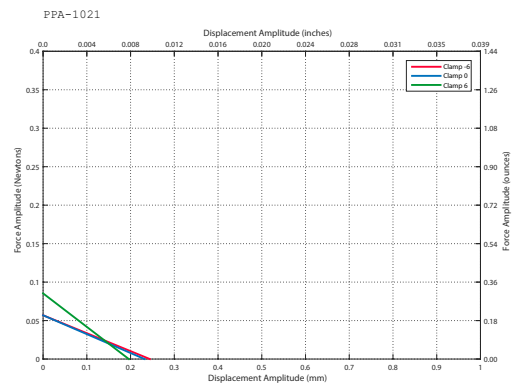


Figure 47: Static displacement and block force are compared for the three different clamp locations. The piezo was driven with 100 volts to generate this data.

Midé Energy Harvester information (4)



2.0 PRODUCT DATA

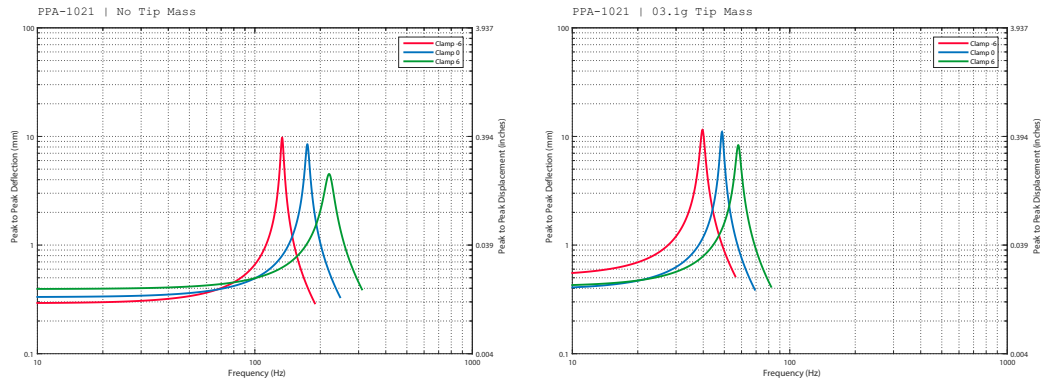


Figure 48: The peak to peak tip displacement is provided for when the piezo is driven with a ± 100 volt signal.

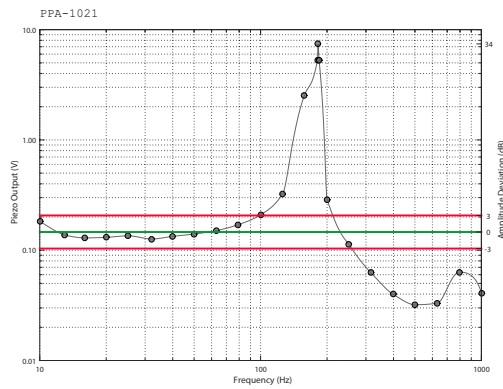
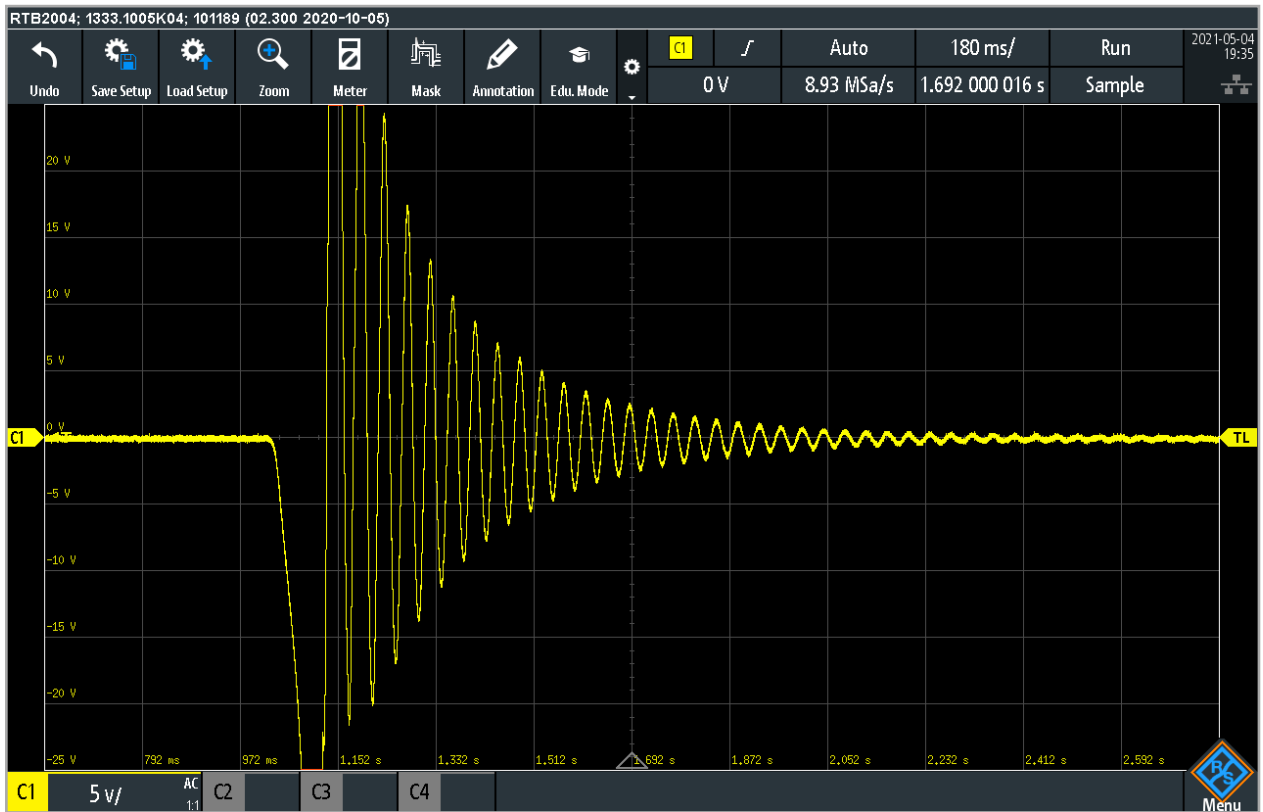
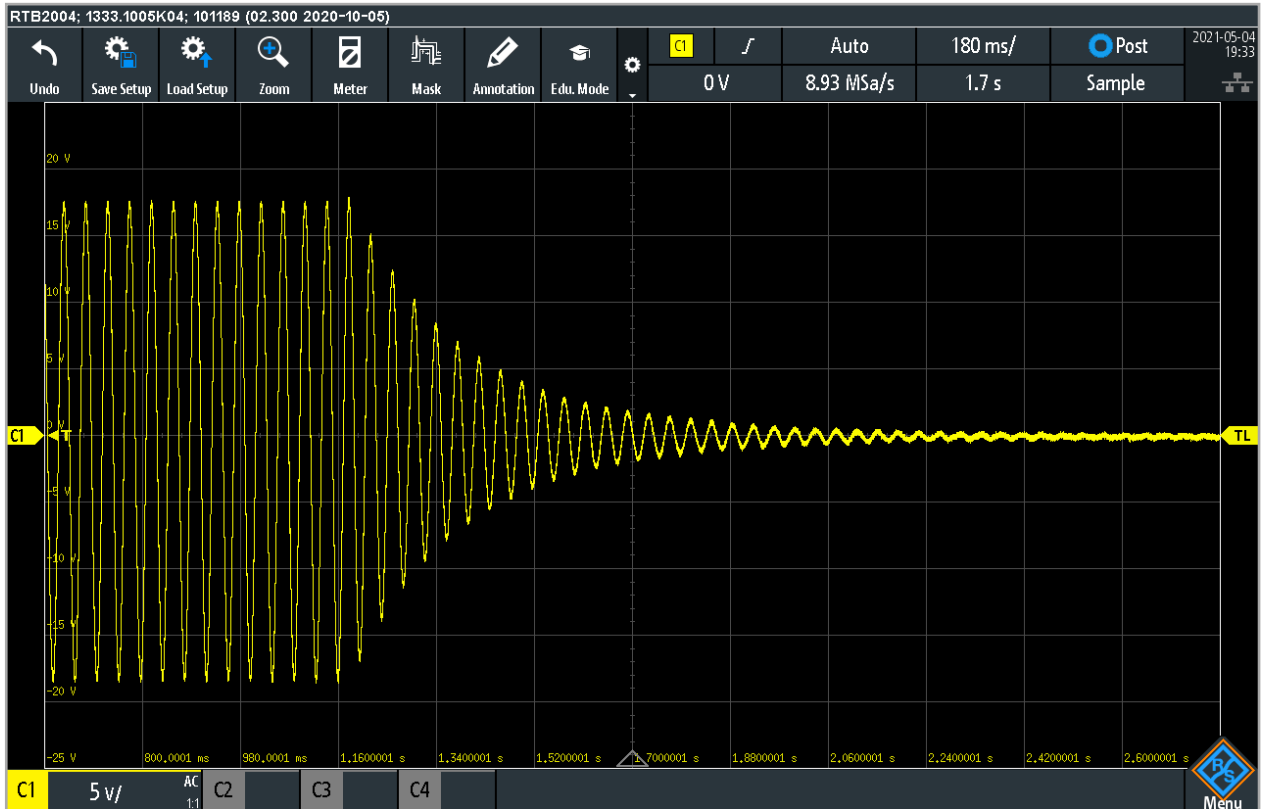


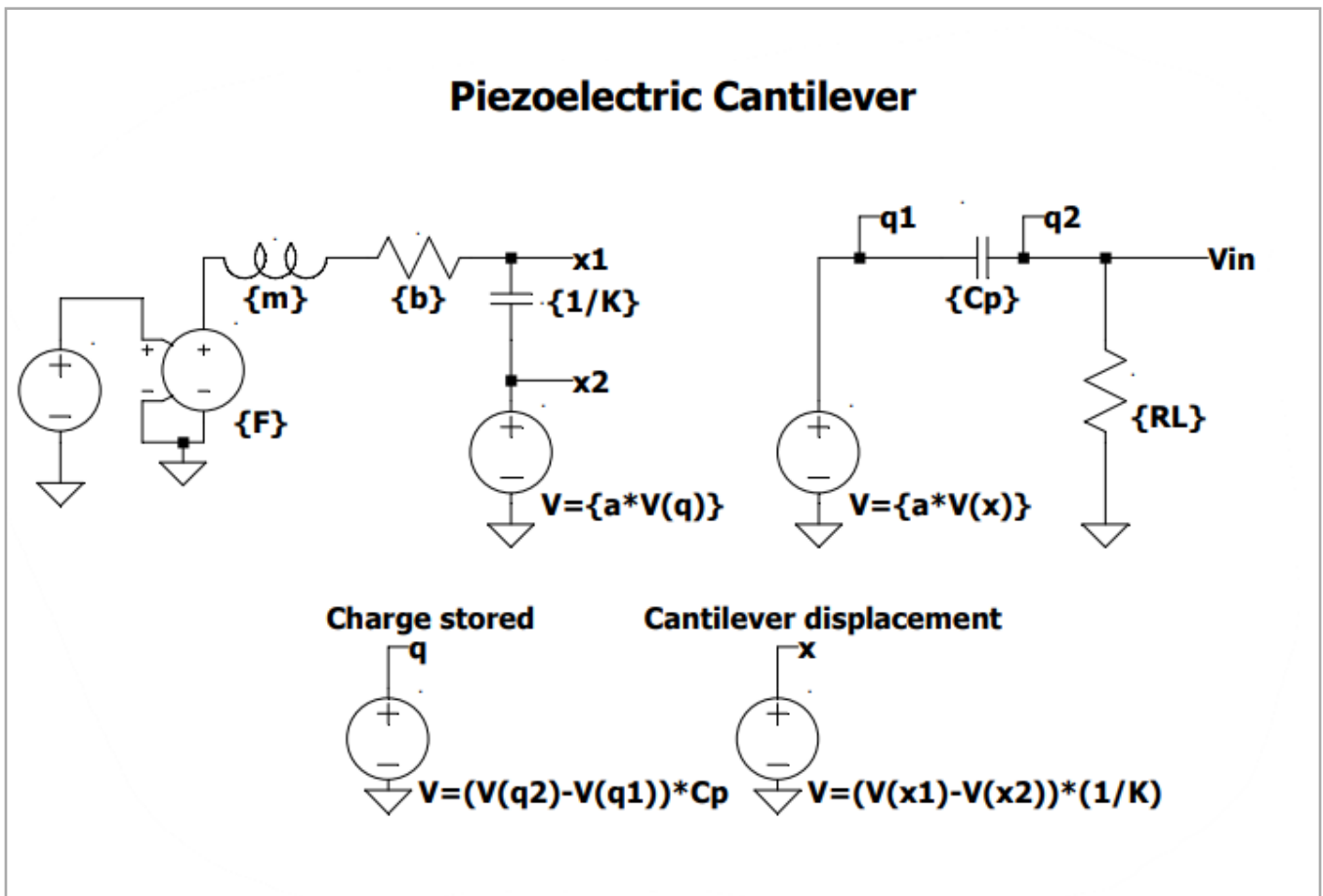
Figure 49: The frequency response of the accelerometer is provided with ± 3 dB error bands to highlight the frequency range where accurate measurement can be expected.



Appendix M: Damping estimations



Appendix N: LTspice circuit



Appendix O: FFT Code (MATLAB)

```

% Accelerometer Analysis
% To witch data file: just change the "1" in "DST1" to "1","2" or "3"
acc_data = load('DST2 Acceleration data 20 Hz.txt');
axxCoeff = 6000/2^15; %resolution coefficient mG's/LSB = 0.183mG's/LSB
xAcc = acc_data(:,5)*axxCoeff;
yAcc = acc_data(:,6)*axxCoeff;
zAcc = acc_data(:,7)*axxCoeff;

%Empty parameters for later use
magAcc = zeros(length(xAcc),1);
theta = magAcc;
phi = theta;
t = zeros(length(xAcc),1);

fs= 20;
N = 0:(length(xAcc)-1);
n = length(N);
T = length(N)*(1/20);

%Computation of resultant
for i = 1:length(xAcc)
    t(i+1) = t(i)+0.05; % @ sample time @ 20Hz
    magAcc(i,1) = sqrt(xAcc(i)^2 + yAcc(i)^2 +zAcc(i)^2);
    theta(i) = atan(xAcc(i)/yAcc(i));
    phi(i) = acos(zAcc(i)/magAcc(i));
end
t = t(1:length(t)-1);

%Resultant corrected for G-vector
magLow = lowpass(magAcc,0.2,fs);
magAcc = magAcc - magLow;

%Fast Fourier Trtansform
X = fftshift(abs(fft(magAcc)));
%X = (abs(fft(magAcc)));
freq = (-fs/2):(fs/(n-1)):(fs/2);
%freq = 0:(fs/(n-1)):(fs);

figure
subplot(2,1,1)
title('Fish Activity')
stem(freq,X/n,'marker','none','color',[32 194 216]/255)
ylim([0 0.2])

ylabel('G's')
xlabel('Frequency [Hz]')

subplot(2,1,2)
plot(t,magAcc,'color',[32 194 216]/255);

xlabel('time [s]')
ylabel('mG's')

```

Appendix P: Chirp and extraction (MATLAB)

```
%Generating Chirp signal
t1=20; % sweep time
fs=1e5; %sampling frequency
f0=1;
f1=50;
t = 0:1/fs:t1;
y = chirp(t,f0,t1,f1);
plot(t,y)
% To generate .wave file for importing into LTSPICE
name='Chirp_(x)Hz_(y)Hz.wav';
audiowrite(name,y,fs)

%Extracting data from dataset B
data = load('axxdata_last.txt');

%Extracting max and average value
Ax_Max=max(data)
Ax_Mean= mean(data)
```

Appendix Q: Voltage and current, simulation (MATLAB)

```
% Simulation operating @ resonance

data = load('ImpedanceSweep.txt');
t = data(:,1);

%Extracting Voltage and current from file
V = data(:,2);
i = data(:,3);

% plotting
plot(t,i*1e6,'LineWidth',1.7,'color',[32 194 216]/255);
grid
title('Operating at 19Hz')
xlabel('Time [s]');
ylabel('Current [\muA]')

figure

plot(t,V,'LineWidth',1.7,'color',[32 194 216]/255);
grid
ylim([-12.5 12.5])
title('Operating at 19Hz')
xlabel('Time [s]');
ylabel('Voltage [V]')
```

Appendix R: Sweep plot (MATLAB)

```
%plotting Sweep Cantilever A nad B
data = load('Sweepfile.txt');
freq = data(:,1);
Slapp = data(:,4);
Stiv = data(:,2);
figure
p1 = plot(freq,Slapp,'color',[32 194 216]/255);
title('Frequency Sweep, Cantilever B')
xlabel('Frequency [Hz]')
ylabel('Voltage [Vrms]')
xlim([4 26])
p1.LineWidth = 1.7;
set(gca,'color',[255 255 255]/255);
grid

figure

p2 = plot(freq,Stiv,'color',[32 194 216]/255);
title('Frequency Sweep, Cantilever A')
xlabel('Frequency [Hz]')
ylabel('Voltage [Vrms]')
xlim([4 26])
p2.LineWidth = 1.7;
set(gca,'color',[255 255 255]/255);
grid
```

Appendix S: Power at resonance (MATLAB)

```

% plotting Voltage, Current and Power Cantilever B @ resonance
data = load('Powersweep.txt');
size (data)
r = data(:,1);
v = data(:,2);
i = data(:,3);
p = data(:,5);

figure
p3 = plot(r,v,'color',[32 194 216]/255)
set(gca,'color',[255 255 255]/255);
xlim([50 1000])
ylim([min(v) 6])
grid
title('Voltage over Potentiometer')
ylabel('Volt [Vrms]')
xlabel ('Resitance [k\Omega]')
p3.LineWidth = 1.7;
figure

p4 = plot(r,i*1e3,'color',[32 194 216]/255)
set(gca,'color',[255 255 255]/255);
xlim([50 1000])
ylim([min(i) 22])
grid
title('Current with Potentiometer')
ylabel('Current (\muA rms)')
xlabel ('Resitance [k\Omega]')
p4.LineWidth = 1.7;
figure

p5 = plot(r,p,'color',[32 194 216]/255)
set(gca,'color',[255 255 255]/255);
xlim ([50 1000])
ylim([min(p) (60)])
title('Power Otput with Potentiometer')
ylabel('Power [\muW]')
xlabel ('Resitance [k\Omega]')
p5.LineWidth = 1.7;
grid

```


Appendix T: Power, different load and accelerations (MATLAB)

```

% Plotting power V acceleration
k100 = [28.8 193.2 339.36];
k200 = [57.06 242.76 435.16];
k300 = [54.26 237.9 420.65];
k400 = [50 218.74 397.66];
k500 = [46 197.66 361.25];
k600 = [41.03 164.1 323.57];
k700 = [38.3 158.6 299.9];
k800 = [28.99 141.7 261.81];
k900 = [28.9 122.5 235.6];
k1000 = [23.5 144.2 215.45];
G = [0.1 0.5 1];
a = 1.9;
plot(G,k100,'LineWidth',a);
hold on
plot(G,k200,'LineWidth',a);
plot(G,k300,'LineWidth',a);
plot(G,k400,':','LineWidth',a);
plot(G,k500,':','LineWidth',a);
plot(G,k600,':','LineWidth',a);
plot(G,k700,'--','LineWidth',a);
plot(G,k800,'--','LineWidth',a);
plot(G,k900,'--','LineWidth',a);
plot(G,k1000,'--','LineWidth',a);
hold off
title('Power Output with different load at varying accelerations')
xlabel('Acceleration');
ylabel('\muW')
legend({'0.1M','0.2M','0.3M','0.4M','0.5M','0.6M','0.7M','0.8M','0.9M','1M'},'
Location','northwest','Orientation','vertical')
grid

```

Appendix U: Accelerometer configuration (Arduino/C)

```

#include <Wire.h>
#include <MPU6050.h>
#include <Statistic.h>

Statistic stats;
MPU6050 mpu;

uint32_t start;
uint32_t stop;

void setup() {

  Serial.begin(115200);
  Serial.println("Initialize Statistics");

  stats.clear(); //explicitly start clean
  start = millis();

  Serial.println("Initialize MPU6050");

  while(!mpu.begin(MPU6050_SCALE_2000DPS, MPU6050_RANGE_2G)){
    Serial.println("Could not find a valid MPU6050 sensor, check wiring!");
    delay(500);
  }

  mpu.setAccelOffsetZ(-887);
  mpu.calibrateGyro();
  checkSettings();
}

void checkSettings() {
  Serial.println();
  Serial.print(" * Accelerometer:          ");
  switch(mpu.getRange()) {
    case MPU6050_RANGE_16G: Serial.println("+/- 16 g"); break;
    case MPU6050_RANGE_8G:  Serial.println("+/- 8 g"); break;
    case MPU6050_RANGE_4G:  Serial.println("+/- 4 g"); break;
    case MPU6050_RANGE_2G:  Serial.println("+/- 2 g"); break;
  }
  Serial.print(" * Accelerometer offsets: ");
  Serial.println(mpu.getAccelOffsetZ());
}

void loop() {
  Vector normAccel = mpu.readNormalizeAccel();
  Vector scaledAccel = mpu.readScaledAccel();

  float absAccel = abs(scaledAccel.ZAxis);

  // Additional manual offset
  stats.add( abs( absAccel-0.02 ) );

  Serial.println(abs(scaledAccel.ZAxis));

  if (stats.count() == 200) {
    stop = millis();
    Serial.println("=====");
    Serial.print("          Count: ");
    Serial.println(stats.count());
    Serial.print("          Min: ");
    Serial.println(stats.minimum(), 4);
    Serial.print("          Max: ");
    Serial.println(stats.maximum(), 4);
    Serial.print("          Average: ");
    Serial.println(stats.average(), 4);
    Serial.print("          time(ms): ");
    Serial.println(stop - start);
    Serial.println("=====");
    stats.clear();
    delay(1000);
    start = millis();
  }

  //delay(20);
}

```

Appendix V: Output from PuTTY

```
COM6 - PuTTY
0.02
0.01
0.02
0.01
0.01
0.02
0.01
0.00
0.02
0.01
0.01
0.02
0.01
0.01
0.01
0.01
0.01
=====
Count: 200
Min: 0.0000
Max: 0.0198
Average: 0.0097
time (ms): 501
=====
```

```
COM6 - PuTTY
0.15
0.12
0.13
0.12
0.10
0.04
0.02
0.09
0.14
0.16
0.19
0.16
0.15
0.12
0.12
0.03
=====
Count: 200
Min: 0.0002
Max: 0.1854
Average: 0.0999
time (ms): 505
=====
```

Appendix W: Poster (A3)

Harvesting of kinetic energy from marine animals

– a poster on piezoelectric generators operating at low frequency vibrations –

OBJECTIVE

Investigate the possibilities of harvesting mechanical energy from fish, and to prove the concept of piezoelectric energy harvesters with a cantilever configuration

GOALS AND MOTIVATION

Prolonging the lifespan of wireless sensor nodes, especially when used for tracking of aquatic animals.

Understand the basics behind piezoelectricity and energy harvesting, and address possible advances in the field.

Be an inspiration for further research.

! FREQUENCY TUNING

IMPOSSIBLE!

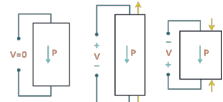


PIEZOELECTRICITY

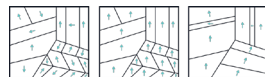
Piezoelectric materials has the ability to convert movement into electricity, and also, to convert electrical input to deflection. This is possible due to the molecular structure of the material:



When the excitation acts on the structure by a pulling force, the positive charged oxygen atoms dominates, and the polarization favours the positive pole. When a force works directly on the atoms, the negatively charged silicon atom dominates, thus, changing the poling.



For the polarization to be fixed, the material needs to be exposed to a strong electric field, which alters the orientation.



It's mathematical ...

ENERGY HARVESTING

One of the most common configurations for vibrations, is the cantilever. This brings us to the biggest challenge of them all. Frequency tuning.



And, of course simulation of a real system with limited degrees of freedom. To be sufficient, the vibrational frequency must match the natural frequency of the system, hence, the fish. Therefore, the resonance must be tuned to 1-3 Hz

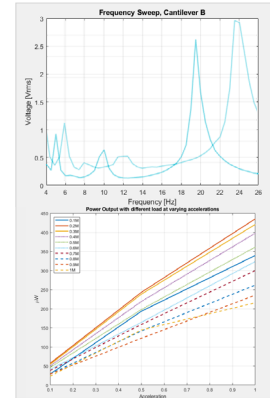
METHOD

... or break the laws of physics ... Either way, the next step is testing, impedance matching, rectifying and storing. And simulations. To simulate this, analogies were needed ... known as the e-v convention. And a few differential equations later, voila ...

$$F = m\ddot{x} + B\dot{x} + kx$$

$$V = L \frac{dq}{dt} + R \frac{dq}{dt} + C^{-1}q$$

RESULTS



CONCLUSION

Piezoelectricity is magic, and like all magic, it's just physics we still do not comprehend. On the field of energy harvesting, there are many unexplored solutions. Let's not quit here :)

Appendix X: AI the supportive rubberduck

